# Computational Bayesian maximum entropy solution of a stochastic advection-reaction equation in the light of site-specific information

Alexander Kolovos, George Christakos, Marc L. Serre, and Cass T. Miller

Center for the Advanced Study of the Environment, University of North Carolina at Chapel Hill, Chapel Hill, North Carolina, USA

Received 29 June 2001; revised 8 May 2002; accepted 8 May 2002; published 28 December 2002.

[1] This work presents a computational formulation of the Bayesian maximum entropy (BME) approach to solve a stochastic partial differential equation (PDE) representing the advection-reaction process across space and time. The solution approach provided by BME has some important features that distinguish it from most standard stochastic PDE techniques. In addition to the physical law, the BME solution can assimilate other sources of general and site-specific knowledge, including multiple-point nonlinear space/time statistics, hard measurements, and various forms of uncertain (soft) information. There is no need to explicitly solve the moment equations of the advection-reaction law since BME allows the information contained in them to consolidate within the general knowledge base at the structural (prior) stage of the analysis. No restrictions are posed on the shape of the underlying probability distributions or the space/time pattern of the contaminant process. Solutions of nonlinear systems of equations are obtained in four space/time dimensions and efficient computational schemes are introduced to cope with complexity. The BME solution at the prior stage is in excellent agreement with the exact analytical solution obtained in a controlled environment for comparison purposes. The prior solution is further improved at the integration (posterior) BME stage by assimilating uncertain information at the data points as well as at the solution grid nodes themselves, thus leading to the final solution of the advection-reaction law in the form of the probability distribution of possible concentration values at each space/time grid node. This is the most complete way of describing a stochastic solution and provides considerable flexibility concerning the choice of the concentration realization that is more representative of the physical situation. Numerical experiments demonstrated a high solution accuracy of the computational BME approach. The BME approach can benefit from the use of parallel processing (the relevant systems of equations can be processed simultaneously at each grid node and multiple integrals calculations can be accelerated significantly, etc.). *INDEX TERMS:* 1829 Hydrology: Groundwater hydrology; 1831 Hydrology: Groundwater quality; 1869 Hydrology: Stochastic processes; *KEYWORDS:* BME, Bayesian, spatiotemporal, advection, reaction, PDE

**Citation:** Kolovos, A., G. Christakos, M. L. Serre, and C. T. Miller, Computational Bayesian maximum entropy solution of a stochastic advection-reaction equation in the light of site-specific information, *Water Resour. Res.*, *38*(12), 1318, doi:10.1029/2001WR000743, 2002.

## 1. Introduction

[2] Modeling techniques generating predictive distributions of contaminant processes across space and time by solving the relevant physical equations have a plethora of applications in environmental sciences [e.g., *Javandel et al.*, 1984; *Knox et al.*, 1993; *Schnoor*, 1996; *Department of Defense*, 1997; *Mynett*, 1999; *Dale and English*, 1999]. Among other things, these techniques offer powerful visual representations of reality in terms of accurate maps of the spatiotemporal distribution of the natural processes of interest. In view of the uncertainty characterizing these distributions, the physical equation usually has the form of a stochastic partial differential equation (PDE). Then, the maps represent the solution of the stochastic PDE given the possibly uncertain boundary/initial conditions of the situation. Two groups of techniques are commonly used for the solution of stochastic PDE: (1) one group focuses on obtaining solutions that are valid for specific realizations of the PDE coefficients (e.g., Monte Carlo or realization-based techniques [*Adler*, 1992; *Spitz and Moreno*, 1996]), and (2) another group is concerned with the estimation of stochastic moments [*Kitanidis*, 1986; *Zhang*, 2002]. Both groups have advantages and drawbacks, and they should be viewed as complementary tools for determining the behavior of stochastic solutions [*Srinivasan and Vasudevan*, 1971; *Jordan and Smith*, 1987; *Flaherty et al.*, 1989].

[3] A different conceptual framework for obtaining stochastic solutions of physical PDE is suggested by the spatiotemporal Bayesian maximum entropy (BME) mapping approach introduced by *Christakos* [1990, 1991] in an epistemic context. In the BME sense, the term "spatiotemporal map" has a broader meaning than usual. In


0043-1397/02/2001WR000743$09.00

particular, the implementation of the BME approach to solve a physical PDE differs from most standard PDE techniques by distinguishing between three main stages of physical knowledge processing and assimilation as follows (Figure 1).

1. At the structural (prior) stage, BME generates an initial probability distribution across space and time based on the physical PDE as well as other forms of general knowledge (primitive equations, multiple-point statistics, etc.), whenever available.

2. At the metaprior stage, databases expressing site-specific states of knowledge (e.g., uncertain observations, new frequency distributions, or empirical charts) are transformed into an operator form suitable for further processing.

3. At the integration (posterior) stage, the initial solution (1) is enriched by assimilating the site-specific data (2). This final solution is not limited to a single realization but includes the complete probability law at each space/time point.

[4] A spatiotemporal map is thus viewed as representing a solution of the physical law in the BME sense (1–3 above). As is proposed by *Christakos* [1992, 2000], in theory two main techniques can be used in stage 1 above: The so-called A technique, which does not need to solve the stochastic moment equations associated with the physical law, whereas the so-called B technique requires the solution of the moment equations. *Christakos and Hristopulos* [1998] examined several theoretical features of these techniques. *Serre and Christakos* [1999] used a numerical approach based on the B technique to study Darcy's law representing groundwater flow in porous media, whereas *Christakos et al.* [1999] combined the B technique with perturbation expansions and diagrammatic analysis. A notable advantage of the A technique over the B technique is that it can be used in cases in which explicit solutions of the moment equations are intractable or the raw moments are not known. By focusing on the B technique, the previous numerical studies left unanswered certain important computational issues related to the efficient implementation of the A technique across space and time. Therefore, in this work we develop a systematic computational approach based on the A technique to solve a stochastic PDE representing the advection-reaction distribution of a pollutant in a river. At the structural BME stage we calculate the general knowledge-based probability density function (PDF) of the pollutant at any point across space and time by numerically solving systems of integrodifferential equations representing the physics of the situation. The obtained results are found to be in excellent agreement with the exact analytical solutions used for comparison. At the metaprior stage we acquire and process different kinds of site-specific knowledge, including hard (accurate) data and soft information in the form of uncertain observations (interval data and probability distributions). At the integration (or posterior) stage the computational BME approach generates with considerable efficiency informative PDF of the contaminant concentration at the nodes of a regular space/time grid. These BME solutions assimilate uncertain information about the contaminant values at the solution nodes themselves, in addition to the measurements available at the data points. The method imposes no restrictions on the shape of the probability laws or the degree of space/time heterogeneity and can account for multiple-point nonlinear statistical moments. Furthermore, BME features more flexible criteria than most standard PDE techniques for choosing the most appropriate, application-dependent solution at each point (i.e., solutions that have the highest probability of occurrence, or satisfy a minimum prediction error criterion, or offer a desired trade-off with regard to certain decision criteria can be chosen, depending on the application).

## 2. Assimilation of General Knowledge by the BME Approach: The Structural (Prior) Stage

### 2.1. Advection-Reaction Law as General Knowledge

[5] In the numerical application presented in this work, the general knowledge (**G**) involves a physical law that governs an advection-reaction process. This law is represented by a PDE and associated initial/boundary conditions [*Weber and DiGiano*, 1996]. The complexity of similar environmental systems often renders them difficult to account deterministically for all the contributing factors in the contaminant process. In that sense, stochastic space/time solutions are reasonably preferred to deterministic model predictions [*Steinberg et al.*, 1996]. More specifically, we consider the temporal evolution of a nondispersive mass transport process along a river, in which case the physical PDE equation describing the space/time distribution of the component mass concentration $X(\boldsymbol{p})$ is as follows

$$\left(\frac{\partial}{\partial t} + q\frac{\partial}{\partial s}\right) X(\boldsymbol{p}) = -\kappa\, X(\boldsymbol{p}), \qquad (1)$$

where $\boldsymbol{p} = (s, t)$ denotes a space/time point ($s$ is the one-dimensional space coordinate along the river direction and $t$ is time), $q$ is the downstream velocity (in $[L]/[T]$), and $\kappa$ is the reaction rate (in $1/[T]$; $\kappa > 0$). In order to account for space/time correlations and random influences, the PDE (1) is considered stochastic, in which case $X(\boldsymbol{p})$ is modeled as a spatiotemporal random field of contaminant concentrations. The boundary/initial condition $X_0 = X(s = 0, t = 0)$ is a Gaussian random variable with mean $\overline{X_0}$ and variance $\sigma_{X_0}^2$, i.e. $X_0 \sim N(\overline{X_0}, \sigma_{X_0}^2)$. In real world applications such a choice is justified on the basis of physical experience (e.g., earlier studies in the area of interest or modeling results offer sufficient insight into the uncertainty of $X_0$ in terms of its probability function). From a research viewpoint, equation (1) is chosen for the additional reason that an exact solution exists, which can serve as a basis of comparison for the solution derived by BME analysis at the structural stage (it is a common practice to test new methods in a controlled environment, since accuracy and consistency cannot in principle be determined on the basis of more "realistic" but complex situations in which the exact solutions are unknown).

### 2.2. General Knowledge-Based PDF Solution

[6] Let the point vector $\boldsymbol{p}_{map} = (\boldsymbol{p}_{data}, \boldsymbol{p}_k)$ denote both the set of $m$ points $\boldsymbol{p}_{data} = (\boldsymbol{p}_1, \ldots, \boldsymbol{p}_m)$ where data are available and the points $\boldsymbol{p}_k$ where stochastic solutions of the PDE (1) are sought (usually on the nodes of a space/time grid). The BME approach generates the prior PDF, $f_G$, at all space/time

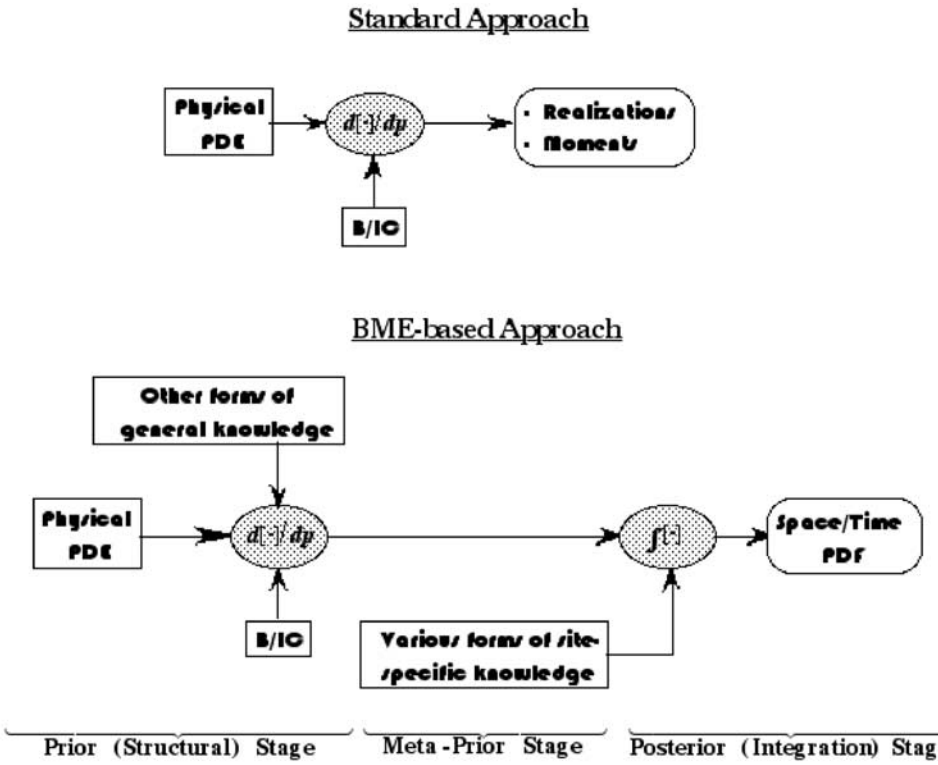


**Figure 1.** Standard and BME-based approaches to studying physical equations. Other forms of general knowledge include empirical relationships, phenomenological laws, and higher-order multiple-point statistics across space and time. Site-specific knowledge includes hard measurements, uncertain (soft) data in the form of intervals, probability functions, fuzzy sets, etc.

points of the vector $\boldsymbol{p}_{map}$ based on the physical law linking these points (the subscript "**G**" in $f_G$ denotes that the probability model has been constructed on the basis of the general knowledge; how this construction is carried out mathematically is discussed by *Christakos* [1998, 2000]). Subsequently, the $f_G$ is conditioned on case-specific data at the integration stage (section 3 below) thus yielding the final PDF, $f_K$, at every grid node $\boldsymbol{p}_k$ where a solution of the PDE is sought (the subscript "K" in $f_K$ means that the probability model has been updated (conditionalized) by means of the site-specific knowledge). According to the BME formulation, in a large number of physical applications the **G** can be expressed in terms of a suitable set of moment equations as follows

$$\overline{h_\alpha}\left(\boldsymbol{p}_{map}\right) = \overline{g_\alpha\left(\boldsymbol{x}_{map}\right)}, \tag{2}$$

where $\alpha = 0, 1, \ldots, N$; the overbar denotes stochastic expectation; $\boldsymbol{x}_{map}$ is the vector of random variables associated with the space/time point-vector $\boldsymbol{p}_{map}$; $h_\alpha$ and $g_\alpha$ are sets of functions the form of which will be determined on the basis of the advection-reaction law (1). Let us set

$$\overline{g_\alpha\left(\boldsymbol{x}_{map}\right)} = \int d\chi_{map}\; g_\alpha\left(\chi_{map}\right) f_G\left(\chi_{map}\right), \tag{3}$$

where $\chi_{map}$ is a realization of the possible concentration values at $\boldsymbol{p}_{map}$. Equation (3) can account for any kind of space/time moments linking the random concentration values at the space/time point vector $\boldsymbol{p}_{map}$. The BME approach permits the incorporation of single-point, two-point and multiple-point moments of any order. As long as these moments are physically obtainable in the context of the available knowledge base, in principle there is no limitation imposed on the multiplicity, the nonlinearity or the order of moments that can be considered by BME. Assume, e.g., that the set of space/time moments available have the general form $\overline{g_a\left(\boldsymbol{x}_{map}\right)} = \prod_i x_i^{\lambda_{i,\alpha}}$, where the $\Pi_i$ denotes product, the $\lambda_{i,\alpha}$ are known integers, and the subscript $i$ can assume any combination of values from the set $\{1, 2, \ldots, m, k\}$; then, the PDF solution produced by BME analysis at the structural stage is given by [*Christakos*, 2000]

$$f_G\left(\chi_{map}\right) = \Lambda \prod_{\alpha=1}^{N} \exp\left[\mu_\alpha \prod_i \chi_i^{\lambda_{i,\alpha}}\right], \tag{4}$$

where $\Lambda = \exp[\mu_0]$, and $\mu_0$ is a normalization constant that accounts for the mathematical constraint that the integral of the PDF is always equal to 1. The calculation of the unknown coefficients $\mu_\alpha$ ($\alpha = 0, 1, \ldots, N$) that are consistent with the physical law is required in order to fully describe the prior PDF $f_G$ in practice.

[7] To obtain some numerical results, we consider space/time points from the point vector $\boldsymbol{p}_{map}$. We require that the moments $\overline{g_\alpha}$ above include the means $\overline{x_i} = \overline{X(\boldsymbol{p}_i)}$, the variances $\sigma_i^2 = \overline{x_i^2} - (\overline{x_i})^2$, and the noncentered covariances $C_{ij} = \overline{X(\boldsymbol{p}_i)X(\boldsymbol{p}_j)}$, or the centered covariances $c_{ij} = C_{ij} - \overline{x_i}\,\overline{x_j}$,

for all points of the vector $\boldsymbol{p}_{map}$. The moments $\overline{g_\alpha}$ must be consistent with the physical law (1) and the information available about the uncertainty of $X_0$ in terms of its statistics. Following the discussion above, equation (2) leads to the following set of equations that is appropriate for our numerical formulation in a controlled environment (Appendix A)

$$\left.\begin{aligned}
&\int\int d\chi_i\, d\chi_j f_G(\chi_i,\ \chi_j) = 1\\
&\int\int d\chi_i\, d\chi_j\, \chi_i \left(\tfrac{\partial}{\partial t_i} + q\tfrac{\partial}{\partial s_i} + \kappa\right) f_G \quad = 0\\
&\int\int d\chi_i\, d\chi_j\, \chi_i^2 \left(\tfrac{\partial}{\partial t_i} + q\tfrac{\partial}{\partial s_i} + 2\kappa\right) f_G \quad = 0\\
&\int\int d\chi_i\, d\chi_j\, \chi_j \left(\tfrac{\partial}{\partial t_j} + q\tfrac{\partial}{\partial s_j} + \kappa\right) f_G \quad = 0\\
&\int\int d\chi_i\, d\chi_j\, \chi_j^2 \left(\tfrac{\partial}{\partial t_j} + q\tfrac{\partial}{\partial s_j} + 2\kappa\right) f_G \quad = 0\\
&\int\int d\chi_i\, d\chi_j\, \chi_i\, \chi_j \left(\tfrac{\partial}{\partial t_i} + q\tfrac{\partial}{\partial s_i} + \kappa\right) f_G = 0
\end{aligned}\right\}, \tag{5}$$

where $f_G = f_G(\chi_i, \chi_j; s_i, t_i, s_j, t_j)$, and it is assumed that the field $X(\boldsymbol{p})$ is differentiable in the mean square sense [*Christakos*, 1992]; the first equation of equation (5) is the normalization condition for the PDF $f_G$. Clearly, a different pair of points from $\boldsymbol{p}_{map}$ will be assigned to a different set of equation (5), etc. In light of the above, the bivariate PDF associated with the pair of points ($\boldsymbol{p}_i$, $\boldsymbol{p}_j$) is a special case of equation (4) as follows

$$f_G(\chi_i,\ \chi_j) = \Lambda^{-1} \exp\left[\mu_1 \chi_i + \mu_2 \chi_i^2 + \mu_3 \chi_j + \mu_4 \chi_j^2 + \mu_5 \chi_i \chi_j\right], \tag{6}$$

where $\Lambda = \exp[\mu_0]$ and $\mu_\alpha = \mu_\alpha(\boldsymbol{p}_i, \boldsymbol{p}_j)$, $\alpha = 0, 1, \ldots, 5$. The form (6) is a result of the decision to account for up to second-order space/time moments, which led to the consideration of single variables and pairs of variables in (6). Coefficients $\mu_\alpha$ are needed at all points of $\boldsymbol{p}_{map}$ to fully define the prior PDF. In this case, the system (5) consists of 6 nonlinear equations, which are discretized and solved numerically with respect to the 6 unknown $\mu_\alpha$ for each pair ($\boldsymbol{p}_i$, $\boldsymbol{p}_j$). If, e.g., we are dealing with $M$ pairs of points from the vector $\boldsymbol{p}_{map}$, we will have $M$ systems of 6 equations each to solve with respect to $6 \times M$ coefficients $\mu_\alpha$. As is expected, each of the $M$ pairs of points is associated with a different $f_G(\chi_i, \chi_j)$. Given the $6 \times M$ coefficients $\mu_\alpha$, the general knowledge-based PDF of the contaminant distribution, $f_G(\boldsymbol{\chi}_{map})$ is obtained from equation (4). Note that an augmented form of (6) would have been used if, e.g., we had decided to consider three-point statistics as well, in which case equation (6) should include triplets of variables ($\chi_i$, $\chi_j$, $\chi_l$); etc. (a similar augmentation is not assumed here, since no exact analytical solutions for the $\mu_\alpha$ values are available in such a case for comparison purposes; see, also, section 2.3 below).

[8] In view of the analysis above, the key element at this stage of the PDE solution procedure is the calculation of the coefficients $\mu_\alpha$. These are first expressed analytically (section 2.3), and then compared to the numerically estimated coefficients in terms of the computational BME approach (section 2.4).

### 2.3. Analytical Expressions for the BME Coefficients

[9] For comparison purposes, the following analytical solution to the advection-reaction equation (1) is considered in terms of contaminant field realizations

$$X(\boldsymbol{p}) = X_0 \exp[-(\kappa - cq)t - cs], \tag{7}$$

where $c$ (in $1/[L]$) is a Gaussian random variable with mean $\bar{c}$ and variance $\sigma_c^2$, i.e., $c \sim N(\bar{c}, \sigma_c^2)$. The physical meaning of $c$ is the inverse of the process characteristic length. The $c$ appears in the temporal component of the realization, as well. Hence we assume randomness in both the spatial and temporal correlation ranges. The analytical solution $f_G$ of the contaminant problem based on equation (7) will be used for comparison with the numerical solution obtained by the proposed computational BME technique at the structural (prior) stage. For this purpose, first we need to find the coefficients $\mu_\alpha$.

[10] More specifically, based on equations (6) and (7) and using well-known properties of the Gaussian probability law (Appendix B), the following exact analytical expressions for the BME coefficients $\mu_\alpha$ ($\alpha = 0, 1, \ldots, 5$) are obtained in terms of the first and second order space/time statistics of the contaminant field for all pairs of points of the vector $\boldsymbol{p}_{map}$,

$$\left.\begin{aligned}
\mu_0\left(\boldsymbol{p}_i,\boldsymbol{p}_j\right) &= -\ln\left(2\pi\sqrt{\vartheta_{ij}}\right) - \left[\overline{x_i^2}\,\sigma_j^2 + \overline{x_j^2}\,\sigma_i^2 - \overline{x_i}\,\overline{x_j}\left(c_{ij} + c_{ji}\right)\right]/2\vartheta_{ij}\\
\mu_1\left(\boldsymbol{p}_i,\boldsymbol{p}_j\right) &= \left[2\left(\overline{x_i}\right)^2\sigma_j^2 - \overline{x_j}\left(c_{ij} + c_{ji}\right)\right]/2\vartheta_{ij}\\
\mu_2\left(\boldsymbol{p}_i,\boldsymbol{p}_j\right) &= -\sigma_j^2/2\vartheta_{ij}\\
\mu_3\left(\boldsymbol{p}_i,\boldsymbol{p}_j\right) &= \left[2\left(\overline{x_j}\right)^2\sigma_i^2 - \overline{x_i}\left(c_{ij} + c_{ji}\right)\right]/2\vartheta_{ij}\\
\mu_4\left(\boldsymbol{p}_i,\boldsymbol{p}_j\right) &= -\sigma_i^2/2\vartheta_{ij}\\
\mu_5\left(\boldsymbol{p}_i,\boldsymbol{p}_j\right) &= \left[c_{ij} + c_{ji}\right]/2\,\vartheta_{ij}
\end{aligned}\right\} \tag{8}$$

where $\vartheta_{ij} = \sigma_i^2\sigma_j^2 - c_{ij}c_{ji}$. The analytical expressions of the means ($\overline{x_i}$, $\overline{x_j}$), variances ($\sigma_i^2$, $\sigma_j^2$) and centered covariances ($c_{ij}$) used in equation (8) are, also, given in Appendix B.

### 2.4. Numerical Solution of the BME System

[11] In this case, the unknown coefficients $\mu_\alpha$ will be the numerical solution of the BME system of equation (5) at every pair of space/time points ($\boldsymbol{p}_i$, $\boldsymbol{p}_j$) from the grid vector $\boldsymbol{p}_{map}$. By substituting equation (6) into (5) we get a system of integro-differential equations (IDE) which are similar to the first kind nonlinear Fredholm IDE [*Goldberg*, 1979]. In our problem we seek a solution of IDE systems where all unknowns are present in every equation. This situation, however, does not fall into any of the well-studied IDE groups. Moreover, the coefficients $\mu_\alpha$ appear in the exponential term of the prior PDF (6) and, as the analytical expression (8) and equation (B4) of Appendix B show, the $\mu_\alpha$ themselves depend on space/time exponentially, as well. The numerical system (5) can be therefore sensitive to fluctuations in the unknown $\mu_\alpha$ values across space and time. Some interesting computational issues related to the solution of system (5) for the coefficients $\mu_\alpha$ are discussed in section 2.5.

[12] In this section, we focus on the results obtained by testing the numerical solution of equation (5) above with the help of an experiment. The numerical experiment considers contaminant leaking at the outfall of a wastewater treatment plant. The origin of the testing area is at initial time $t_0 = 0$ (in days) and location $s_0 = 0$ (in km) along the downstream direction, and the advection-reaction process is governed by the law (1). Water velocity $q$ and reaction rate $\kappa$ are assumed

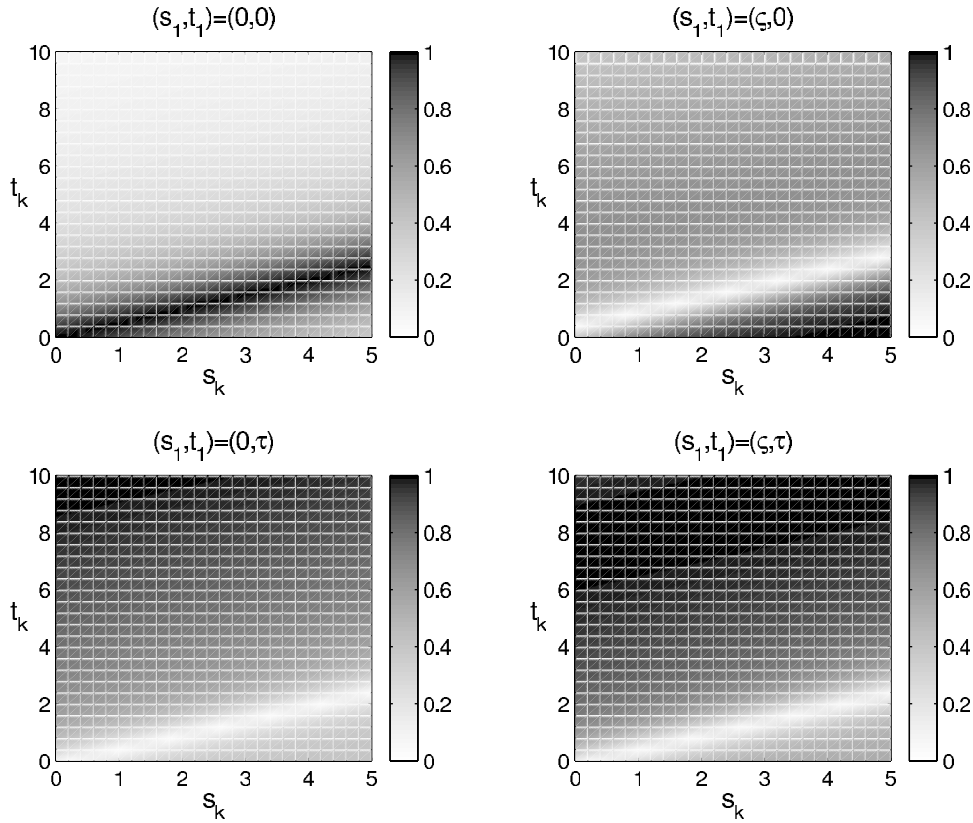


**Figure 2.** Patterns of the absolute value of the correlation coefficient ($|\rho_x|$) between four selected data nodes and the mapping domain in space/time.

constants. Any number of data points and solution nodes can be processed by the computational BME technique. However, for numerical illustration purposes we examined two controlled environments: the first environment assumed a single datum, whereas the second environment involved a cluster of data points.

**2.4.1. One Datum Point and a Grid of Solution Nodes**

[13] In this case we used a 4-D grid consisting of two separate subgrids: One of them contains a single point $\boldsymbol{p}_1$ and the other one includes all solution nodes $\boldsymbol{p}_k$ (also called, estimation points); these two subgrids may be arbitrarily located in space/time. Different space/time origins and grid parameters were assumed for each one of the subgrids. The values assigned to the physical problem parameters are shown in the upper part of Table 1 (lines 2–7). The numerical properties of the proposed technique were investigated assuming a resolution of $N_\tau = 200$ nodes in the temporal domain. The resolution of the spatial domain, $N_\varsigma$, is then derived with the help of the CFL condition: see equation (10). Focusing on a soft datum at $\boldsymbol{p}_1$ = (0.1 km, 0.05 days) and using the parameters values of the lower part of Table 1 (lines 8–23), we solved for the coefficients $\mu_\alpha(\boldsymbol{p}_1, \boldsymbol{p}_k)$ at each node $\boldsymbol{p}_k$ of a numerical grid with $N_{s_1} \times N_{t_1} \times N_{s_k} \times N_{t_k} = 1 \times 1 \times N_\varsigma \times N_\tau = 1 \times 1 \times 50 \times 200$ nodes: a total of 10,000 nodes. The correlation between the points $\boldsymbol{p}_1$ and $\boldsymbol{p}_k$ exhibits a pattern that depends on both the relative location of the points and the physical problem itself. The correlation coefficient is given by

$$\rho_{1k} = c_{1k} / \sigma_1 \sigma_k. \tag{9}$$

For illustration, Figure 2 depicts the emerging space/time correlation patterns by plotting the $|\rho_{1k}|$ values on the solution subgrid, for four possible locations of the data point ($\boldsymbol{p}_1$). The plots used the exact values of the variances and covariance of the random concentration field (Appendix B). The physical behavior shown in Figure 2 requires some

**Table 1.** The Parameters and the Values Used in Our Study

| Parameter | Symbol | Value |
|---|---|---|
| Downstream velocity | $q$ | 2 km day$^{-1}$ |
| Reaction rate | $\kappa$ | 0.5 day$^{-1}$ |
| Initial concentration mean | $\overline{X_0}$ | 10 ppm |
| Initial concentration variance | $\sigma_{X_0}^2$ | 2 ppm$^2$ |
| Mean of parameter $c$ | $\bar{c}$ | 0.2 km$^{-1}$ |
| Variance of parameter $c$ | $\sigma_c^2$ | 0.005 km$^{-2}$ |
| Temporal domain size | $\tau = \lvert\kappa - \bar{c}q\rvert^{-1}$ | 10 days |
| Spatial domain size | $\varsigma = 1/\bar{c}$ | 5 km |
| Resolution in $\tau$-domain | $N_\tau$ | 200 nodes |
| $t_1$ temporal nodes in grid | $N_{t_1}$ | 1 |
| $t_k$ temporal nodes in grid | $N_{t_k}$ | $N_\tau$ |
| Temporal step | $\delta t_1 = \tau/N_\tau$ | 0.05 days |
| Temporal step | $\delta t_k$ | $\delta t_1$ |
| Spatial step | $\delta s_1 = \lvert q\ \delta t_1\rvert$ | 0.1 km |
| Spatial step | $\delta s_k$ | $\delta s_1$ |
| Resolution in $\varsigma$-domain | $N_\varsigma = \varsigma/\delta s_1$ | 50 nodes |
| $s_1$ spatial nodes in grid | $N_{s_1}$ | 1 |
| $s_k$ spatial nodes in grid | $N_{s_k}$ | $N_\varsigma$ |
| Spatial origin in ($s_1$, $t_1$) | $s_{1_0}$ | 0 km |
| Temporal origin in ($s_1$, $t_1$) | $t_{1_0}$ | 0 days |
| Spatial origin in ($s_k$, $t_k$) | $s_{k_0}$ | 0 km |
| Temporal origin in ($s_k$, $t_k$) | $t_{k_0}$ | 0.4 $\tau$ = 4 days |

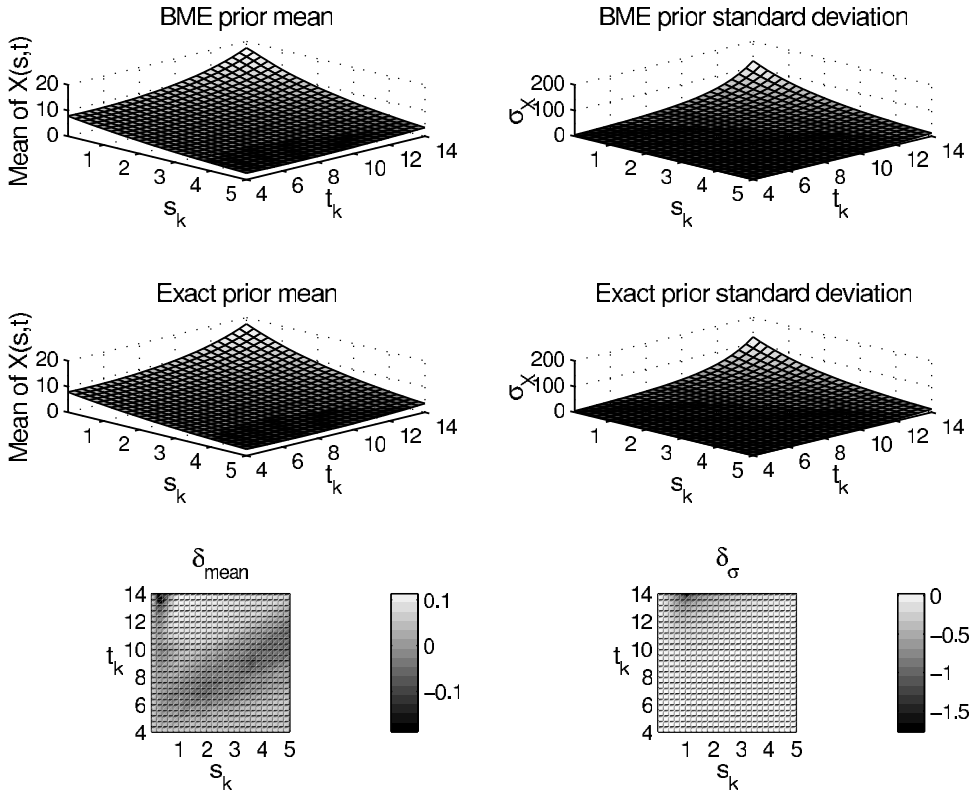


**Figure 3.** BME calculated versus analytical (exact) prior mean $\bar{x}$, standard deviation $\sigma_x$ and estimation errors, $\delta_{\text{mean}} = \bar{X}_{Exact} - \bar{X}_{BME}$, and $\delta_\sigma = \sigma_{Exact} - \sigma_{BME}$.

attention when solving the numerical system (5). At the space/time points where $\rho_{1k} \approx 1$ the bivariate PDF, $f_G(\chi_1, \chi_k)$, displays singular behavior, since the corresponding covariance matrix determinant tends to zero. This behavior is expected when the points $\boldsymbol{p}_1$ and $\boldsymbol{p}_k$ are close to each other (in the special case $\boldsymbol{p}_1 = \boldsymbol{p}_k$, the bivariate PDF degenerates to a univariate PDF). Figure 2 suggests that there may exist high correlation regions even when $\boldsymbol{p}_1$ and $\boldsymbol{p}_k$ are at a considerable distance from each other (which may be due to the advective form of equation (1)).

[14] The numerical estimates of the $\mu_\alpha$ coefficients showed an excellent agreement with the exact analytical values. Another indicator of the effectiveness of the solution technique is obtained by using the numerical $\mu_\alpha$ values to map the prior BME mean and standard deviation of the contaminant across space/time. In Figure 3 these BME maps are compared to the exact prior mean and standard deviation. The corresponding error plots (numerical versus exact values) of the mean and standard deviation, $\delta_{mean} = \overline{x_{Exact}} - \overline{x_{BME}}$ and $\delta_\sigma = \sigma_{Exact} - \sigma_{BME}$, respectively, are also shown. Note that the maxima of these errors correspond to 1% of the exact value at most, which demonstrates the high solution accuracy of the computational BME technique. The results of the numerical experiment were compared with these obtained for a finer grid. It was found that the concentration means and variances for the finer grid are almost the same as those previously obtained for the coarser grid, whereas the system's root convergence behavior was not affected by the use of a finer discretization.

[15] Furthermore, a sensitivity analysis was conducted for perturbed values of the physical parameters of the problem ($q$, $\kappa$, $\overline{X_0}$, $\sigma_{X_0}^2$, $\bar{c}$, and $\sigma_c^2$). The numerical experiment was repeated assuming a resolution of $N_\tau = 200$ nodes along the time direction using the new values of the physical parameters in Table 2. During each repetition of the experiment we perturbed only one of the 6 physical parameters (the others were kept unchanged). The domain sizes (determined by $\varsigma = \bar{c}^{-1}$ and $\tau = |\kappa - \bar{c}q|^{-1}$ in space and time, respectively) were changed accordingly. For example, an increased river velocity results in a reduction of the temporal correlation size. The variance of $c$ showed some sensitivity that might affect the PDE solution of contaminant concentration, especially when the data points and the solution nodes are separated by large space/time distances. The larger the $\sigma_c^2$ is, the larger is the concentration mean at distant solution nodes. Mathematically, this behavior is explained by the presence of $\sigma_c^2$ in the exponential term of the analytical expression for the concentration mean (Appendix B). Physically, a larger $\sigma_c^2$ value implies that higher contaminant concentrations dominate lower ones at remote locations (this effect is displayed in Figure 9a). Minor changes were also observed in the correlation coef-

**Table 2.** Modified Values That Were Tested for the Physical Parameters of the Problem

| Parameter | Symbol | Perturbed Value |
|---|---|---|
| Downstream velocity | $q$ | 4 km day$^{-1}$ |
| Reaction rate | $\kappa$ | 0.25 day$^{-1}$ |
| Initial concentration mean | $\overline{X_0}$ | 20 ppm |
| Initial concentration variance | $\sigma_{X_0}^2$ | 1 ppm$^2$ |
| Mean of parameter $c$ | $\bar{c}$ | 0.4 km$^{-1}$ |
| Variance of parameter $c$ | $\sigma_c^2$ | 0.01 km$^{-2}$ |

ficient ($|\rho_{1k}|$) profiles, since correlation between points $\boldsymbol{p}_1$ and $\boldsymbol{p}_k$ is affected by changes in the values of the physical parameters. However, the numerical behavior of system (5) remained overall unaffected, and the solutions were accordingly regulated by the new parameter values.

#### 2.4.2. Clusters of Data Points and Solution Grid Nodes

[16] In this case the space/time data points ($\boldsymbol{p}_{data}$) formed a cluster and the solution nodes ($\boldsymbol{p}_k$) formed a regular grid. The physical parameters are the same as in the preceding case 1. However, we now have a 4-D grid of $N_{s_1} \times N_{t_1} = 6 \times 60$ data nodes in space/time and $N_{s_k} \times N_{t_k} = 10 \times 40$ solution nodes: a total of 144,000 nodes. Table 3 shows the current choice of grid parameters which differ from their counterparts in Table 1. The new grid parameters have been selected taking into account the increased grid size used in this case. As in case 1, numerical instability problems were avoided by selecting configurations of data points and solution grid nodes that do not exhibit correlation values close to 1. By iterating over these nodes, solutions for the corresponding $\mu_\alpha$ coefficients were derived at the prior BME stage. The numerical results obtained in this case are of similar accuracy as those obtained in case 1. A relevant plot based on the results of case 2 will be shown (in Figure 8).

**Table 3.** Parameters Taken Different in Case 2 Than Shown in Table 1

| Parameter | Symbol | Value |
|---|---|---|
| $t_1$ temporal nodes in grid | $N_{t_1}$ | 60 |
| $t_k$ temporal nodes in grid | $N_{t_k}$ | 40 |
| $s_1$ spatial nodes in grid | $N_{s_1}$ | 6 |
| $s_k$ spatial nodes in grid | $N_{s_k}$ | 10 |
| Spatial origin in ($s_1$, $t_1$) | $s_{1_0}$ | 0 km |
| Temporal origin in ($s_1$, $t_1$) | $t_{1_0}$ | 0 days |
| Spatial origin in ($s_k$, $t_k$) | $s_{k_0}$ | 0.4 $\varsigma$ = 20 km |
| Temporal origin in ($s_k$, $t_k$) | $t_{k_0}$ | 0.6 $\tau$ = 4 days |

### 2.5. Computational Issues

#### 2.5.1. On the Numerical Solution of the BME System

[17] A Newton-Raphson nonlinear solver was used for the solution of the system of equation (5). There exist several variants of this method based on Newton's root finding scheme [*Conte and De Boor*, 1980]. These variants can be helpful with respect to case-specific issues, e.g., when the parameter does not always converge to the solution or when the derivatives of the system's coefficients can not be expressed explicitly. Regarding the latter issue, an indirect calculation of the derivatives may lead to increased iterations, thus reducing cost effectiveness. The calculation of these derivatives is often a reason for choosing other iterative methods, e.g., secant methods in which derivatives are approximated by differences [*Ortega and Rheinboldt*, 1982]. In the present case the derivatives of the coefficients $\mu_\alpha$ are derived directly from (5); the discretized system of equations is presented later. Convergence of the Newton-Raphson technique toward a solution is an important factor that depends on the degree of proximity of the initial guess to the true value [*Atkinson*, 1989]. This factor can create some difficulties in obtaining numerical solutions when dealing with sensitive systems, such as equation (5). For example, the Newton-Raphson step may overshoot the iteration solution away from the actual root, thus misdirecting the system to unstable regions. An additional degree of complexity stems from the elaborate form of equation (5), in which case the existence of multiple local minima in the solution domain is a realistic possibility. The standard Newton-Raphson method advances with equal-sized steps, and if drawn into the area of local minima it may lock around one of them failing to converge to the actual root. To remedy the situation we adopted a globally converging Newton-Raphson algorithm based on line searching and backtracking along the solution gradient that utilizes steps of variable sizes [*Nocedal and Wright*, 1999]. Given the sensitivity of the system unknowns with respect to changes in the space/time variables, numerical tests showed that the system makes intense use of the line search procedure to achieve convergence to the actual root (with a negligible computational cost). For additional support, we refined the initial guess at each space/time step by using an equally weighted mean of the calculated $\mu_\alpha$ values at the closest neighboring nodes visited in previous iterations, thus leading to very satisfactory numerical results.

##### 2.5.1.1. The 4-D Stencil

[18] We are dealing with a 4-D problem in space/time, which presents some interesting computational modeling challenges. Typical multidimensional problems display one or more spatial dimensions plus time, whereas in our case it is required to consider equations in pairs of points from $\boldsymbol{p}_{map}$. To discretize equation (5), we propose a physical interpretation of the problem as follows: Based on the fact that we are dealing with two-point statistics, the 4-D discretization system ($s_i$, $t_i$, $s_j$, $t_j$) is viewed as the cross-product, ($s_i$, $t_i$) $\times$ ($s_j$, $t_j$), of two 2-D subsystems (Figure 4a). In this way, $\boldsymbol{p}_i = (s_i, t_i)$ and $\boldsymbol{p}_j = (s_j, t_j)$ are seen as two interacting but physically separated subsystems in space/time (this approach also allows for a meaningful extension to more than two points, when one decides to consider multiple-point statistics). A convenient graphical representation of the above arrangement is given in Figure 4b by means of a 3-D cube ($s_i$, $t_i$, $s_j$) evolving in time $t_j$. The coefficients $\mu_\alpha(\boldsymbol{p}_i, \boldsymbol{p}_j)$ are then discretized with respect to each of the subsystems used.

##### 2.5.1.2. Discretization Scheme

[19] An explicit scheme is used to solve system (5) for each pair of points ($\boldsymbol{p}_i$, $\boldsymbol{p}_j$). A variety of discretization schemes exists, some of which focus on advective transport PDE [e.g., *Farthing and Miller*, 2000]. Although the physical law (1) is expressed as a stochastic PDE, in this work we are not solving a typical PDE problem. As a result, a physical interpretation of the problem is helpful in making a sensible choice of the discretization scheme. In particular, system (5) consists of functionals in which the law (1) is embedded. Since (5) is essentially a functional form of equation (1), it displays key characteristics of the particular family of equations that (1) belongs to, namely, the family of hyperbolic PDE. We subsequently selected the first-order accurate Lax-Friedrichs scheme, commonly used in the explicit solution of hyperbolic PDE [*Strikwerda*, 1989], as the discretization scheme for equation (5). The process of discretizing the BME system (5) and obtaining algebraic expressions for the equations and their derivatives is presented in Appendix C. A simplified schematic representation of the 4-D stencil arising from this discretization is

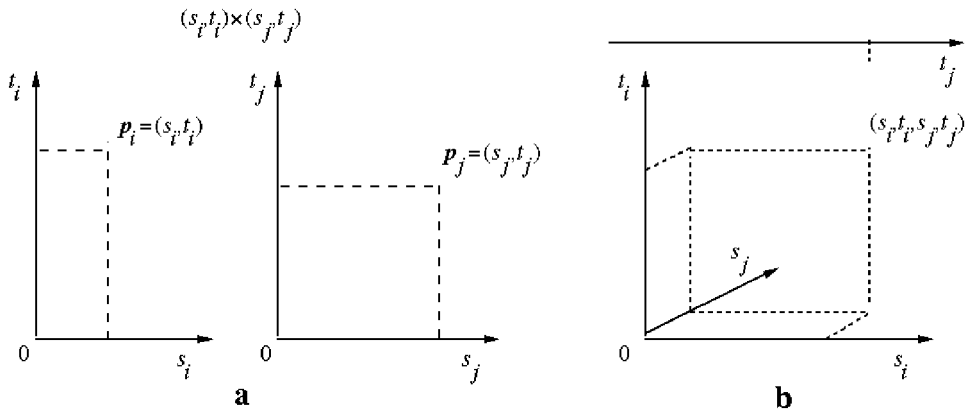


**Figure 4.** The four-dimensional (4D) representation of the numerical problem may be depicted graphically either as (a) the cross-product between the 2D spaces ($s_i$, $t_i$) × ($s_j$, $t_j$) or (b) as a 3D cube ($s_i$, $t_i$, $s_j$) evolving with time $t_j$.

shown in Figure 5. Regarding the numerical boundary/initial conditions, the Lax-Friedrichs scheme requires knowledge of all variable values at the initial times ($t_i = t_j = 0$) as well as at the lower (upstream) spatial boundaries. Schematically, using Figure 4b this translates into requiring knowledge of the coefficients $\mu_\alpha$ at every node in the first space/time cube, as well as the face-nodes on the remaining cubes that correspond to $t_i = s_i = s_j = 0$.

[20] Our earlier comments, namely that equation (5) display hyperbolic PDE characteristics, are supported by numerical findings and experiments. For example, our tests showed that root-finding inaccuracies due to a poor initial guess propagate in the form of discontinuities throughout the stencil (a similar situation can be, also, observed in hyperbolic PDE solutions [*Lapidus and Pinder*, 1982]). As is the case with any hyperbolic system, the Courant-Friedrichs-Lewy (CFL) condition

$$R = |v\Delta t/\Delta s_i| \leq 1 \tag{10}$$

was enforced to assure stability of the PDE numerical solution along the spatial discretization direction $s_i$, where $v$ is a characteristic speed that can be either a constant or a variable. We adopted the equality relationship in equation (10), which keeps numerical dispersion and dissipation small in the solution of hyperbolic PDE [*Strikwerda*, 1989].

### 2.5.2. Performance and Numerical Integration

[21] At each node ($s_i$, $t_i$, $s_j$, $t_j$) of the 4-D discretization grid, the numerical problem of solving for $\mu_\alpha(\boldsymbol{p}_i, \boldsymbol{p}_j) = \mu_\alpha(s_i, t_i, s_j, t_j)$, $\alpha = 0, 1, \ldots, N$ ($N = 5$ in the case of equation (5)) requires the following computational effort: (1) $N$ function calculations plus 1 for the normalization condition, whereas the $\mu_0$ is calculated as a function of the remaining $N$ coefficients; (2) $N^2$ derivatives for the Jacobian matrix with respect to the unknown coefficients; and (3) solution of a $N \times N$ linear system at each Newton-Raphson iteration. At each node of the space/time grid, the nonlinear solver approaches the root fast (convergence is normally achieved within only a few Newton-Raphson iterations). The main computational cost lies in the calculation of the double integrals of system (5) and its Jacobian. We have used an efficient integration method, namely, a 32-point Gauss-Legendre Quadrature (often referred in the literature as GQ) with adaptive integration limits [*Atkinson*, 1989] (see also section 2.5.2.1). The GQ was found to outperform by a full order of magnitude Newton-Cotes-based integration formulas for the same accuracy level in single integral calculation tests.

#### 2.5.2.1. Integrating Intervals

[22] An adequate understanding of the behavior of the physical system requires the consideration of a numerical grid that extends to at least one characteristic length in space and one in time. However, the randomness of the inverse correlation length $c$ does not allow the exact knowledge of these quantities. Therefore they are approximated using a spatial subdomain of size $\varsigma = \bar{c}^{-1}$ (in [$L$]) and a temporal subdomain of size $\tau = |\kappa - \bar{c}q|^{-1}$ (in [$T$]). The numerical processing of this task is inherently serial, i.e., one needs to know values at previously visited nodes in order to advance through the grid. We take advantage of this property to select adaptive integration limits as follows: The integration intervals are set with respect to the means and variances calculated for the previously visited grid node. Tchebyscheff's inequality [*Papoulis*, 1991] is used to find values of the integration variables $\chi_i$ and $\chi_j$ around their respective means where the integrands in (5) are nonzero. Following this approach in a series of numerical integration tests we found that for intervals ranging within 6 standard deviations or more around the means at a set of points, the numerically calculated double integral retained a nine digit accuracy. The intervals on the starting grid node were obtained through the boundary/initial conditions assumed.

#### 2.5.2.2. Parallel Processing

[23] The computational performance of BME can be improved by using parallel processing (e.g., multigrid techniques are often applied to elliptic PDE that allow parallel processing of small-sized grids by decomposing the original stencil [*McCormick*, 1987; *Smith et al.*, 1996]). The BME-based code's performance was improved with the help of rudimentary tests implementing parallel processing. Code profiling showed that a larger amount of execution time (almost 14%) is spent on double integration, whereas about 8.5% of the time is spent for the calculation of exponential functions. The 5 function calculations involved

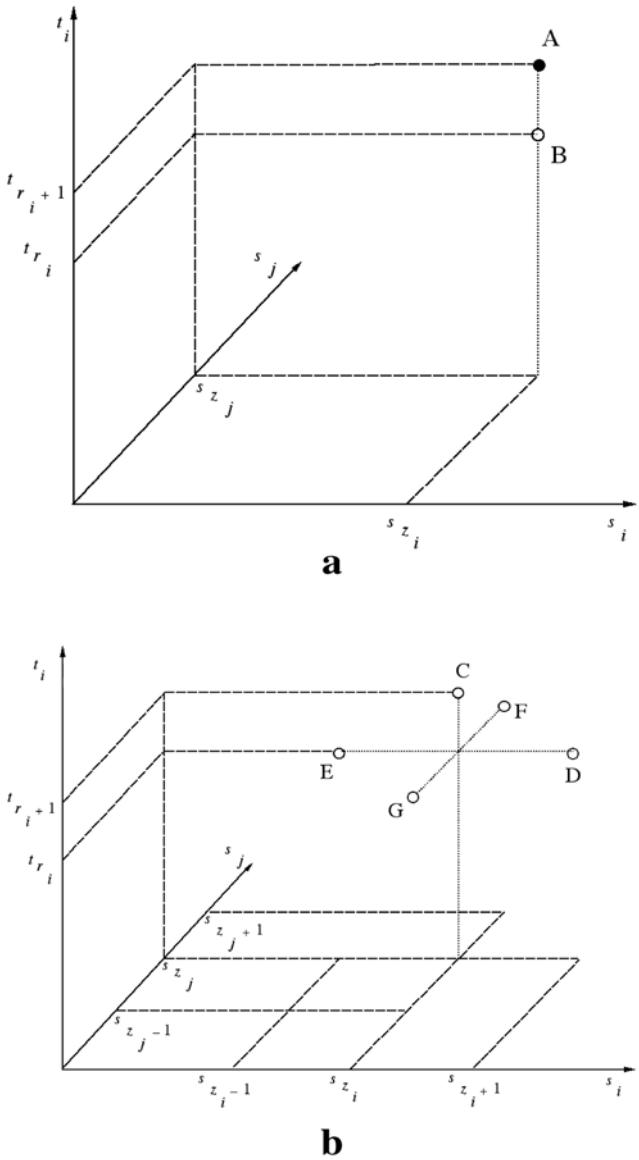


**Figure 5.** Representation of the discretization stencil in the 4D space ($s_i$, $t_i$, $s_j$, $t_j$) depicted as a cube ($s_i$, $t_i$, $s_j$) evolving with time $t_j$. Using the symbolism in Appendix C, the solid circle A in Figure 5a represents the node at which numerical solution is sought for the unknowns $\mu_{\alpha_{z_i,z_j}}^{r_i+1,r_j+1}$ ($\alpha$ = 0, 1, …, 5). The open circles denote grid nodes where the coefficients $\mu_\alpha$, ($\alpha$ = 0, 1, …, 5) are known. In particular, Figure 5a depicts the nodes A and B (corresponding to $\mu_{\alpha_{z_i,z_j}}^{r_i,r_j+1}$) where values are taken at $t = t_{r_j+1}$; in Figure 5b we show the nodes used at time $t = t_{r_j}$, i.e., the values of $\mu_{\alpha_{z_i,z_j}}^{r_i+1,r_j}$ at C, $\mu_{\alpha_{z_i+1,z_j}}^{r_i,r_j}$ at D, $\mu_{\alpha_{z_i-1,z_j}}^{r_i,r_j}$ at E, $\mu_{\alpha_{z_i,z_j+1}}^{r_i,r_j}$ at F, and $\mu_{\alpha_{z_i,z_j-1}}^{r_i,r_j}$ at G.

in equation (5) follow with about 7% each, and their 25 derivatives calculations trail at around 1.3% of cpu time each. Accordingly, we addressed the potential of parallelizing some of these processes. Two different tests were conducted in which we used the MPI standard [*Gropp et al.*, 1999] and 6 SGI Origin 2000 processors to run parallel jobs. In the first test, we focused on parallelizing the double integration in $\chi_i$ and $\chi_j$ and distributed the load to 4 processors. The main test application ran in parallel on average 2.86 times faster than the serial execution on the same machine (compared to an expected linear speed-up factor of 4 using as many processors). On the other hand, in the second parallel processing test we distributed the load of calculating the functions and their derivatives to multiple processors. The code was rearranged so that each one of 5 processors was assigned to calculate a function and its derivatives throughout the Newton-Raphson call at a given ($\boldsymbol{p}_i$, $\boldsymbol{p}_j$) stencil node. We mentioned earlier that the code spends considerable time inside the functions and the derivatives (in fact, this could cumulatively occupy about 70% of the execution time). By splitting this load onto 5 different processors we found that the code performs on the average 2.7 times faster than the serial execution time required on the same machine. These tests clearly demonstrate that, even at an elementary level the proposed BME method is open to computational parallelization that improves its performance considerably compared to serial processing.

## 3. Assimilation of Site-Specific Knowledge by the BME Approach: Metaprior and Integration (Posterior) Stages

[24] Following the general knowledge (**G**) assimilation stage is the metaprior stage at which the site-specific knowledge (**S**) is gathered and evaluated (Figure 1). In principle, **S** includes accurate real-time measurements and experimental outcomes which constitute the hard data body, as well as several types of uncertain observations represented as soft data. At the final (posterior or integration) stage, these two knowledge bases are combined (K = G ∪ S) and logically processed to yield the final PDF ($f_K$) and predicted contaminant concentrations at the solution nodes of the space/time domain. Hence, by deriving the complete PDF of the contaminant field at each grid node $\boldsymbol{p}_k$, the BME method goes further than merely obtaining a solution for the stochastic PDE (1) in the usual (realization or statistical moment) sense. In deriving the solutions $f_K$ we will use not only general knowledge (the advection-reaction law) but all available site-specific knowledge, as well (it will be shown below that **S** takes various forms, one of which is uncertain information at the solution grid nodes themselves).

[25] Two sorts of soft data commonly encountered at the metaprior stage are as follows: (1) measurements within an interval of uncertainty large enough so that they cannot be considered as unique hard data; and (2) information available in the form of case-specific probability densities $f_S(\chi_{soft})$. In these two cases the corresponding total knowledge (K)-based PDF at the integration stage are given by [*Christakos*, 1998]

$$f_K(\chi_k) = A^{-1} \int_I d\chi_{soft} f_G(\chi_{soft}, \chi_k) \tag{11}$$

and

$$f_K(\chi_k) = A^{-1} \int d\chi_{soft} f_S(\chi_{soft}) f_G(\chi_{soft}, \chi_k) \tag{12}$$

respectively, where $I$ is the soft interval domain and $A$ is a normalization operator. Assimilation techniques for a

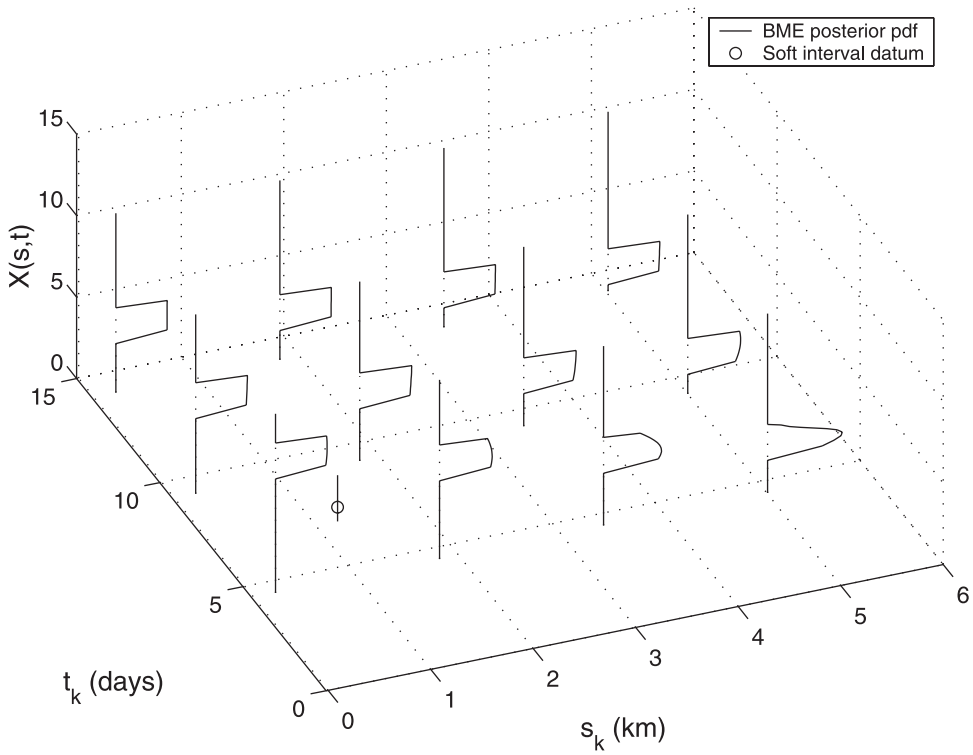


**Figure 6.** Interval (soft) datum at point $\boldsymbol{p}_1$ = (0.1 *Km*, 0.05 *Days*) and BME posterior PDF at several solution grid nodes $\boldsymbol{p}_k$ with interval soft data.

variety of other soft (uncertain) data types, as well as insight about multipoint BME solutions are given by *Christakos* [2000].

[26] In light of equations (11) and (12), the stochastic solution ($f_G$) of the physical equation (1) obtained earlier is updated by using site-specific interval and probabilistic data to condition the prior PDF, thus leading to the new PDF $f_K$. As before, for numerical illustration an interval datum was assumed at the space/time point $\boldsymbol{p}_1$ = 0.1 km, 0.05 days. This interval datum was created as follows: First, concentrations were generated by a random field simulator based on equation (7) with random $X_0$ and $c$ values drawn from the respective probability laws. Then, each simulated value $\zeta$ was randomly placed within an interval of uniformly distributed values around $\zeta$, thus creating the desired interval datum. Moreover, indirect information about the contaminant is often available, say, in the form of a locally valid tracer experiment. Such information is viewed as an additional soft datum at each solution node. For example, Figure 6 shows an interval datum at $\boldsymbol{p}_1$ together with the BME-based $f_K$ at 12 selected solution nodes in the region where $f_G$ was calculated earlier. These $f_K$ (which show a variety of different shapes) have been conditioned on the local soft datum at $\boldsymbol{p}_1$ as well as on the soft data available at the solution nodes (the $f_K$ plots in Figure 6 have been properly scaled).

[27] Figure 7 displays a series of space/time $f_K$ which differ from the PDF of Figure 6 in two ways: (1) Figure 7 is concerned with the case of probabilistic site-specific data, instead of interval data. This situation may arise, e.g., when there exists a series of measurements at a point or when the soft datum is the result of some fitting procedure. In this numerical experiment we assumed knowledge of the measurement mean (in ppm) at each solution node (obtained from simulated values at the soft datum point) and a common measurement variance (0.1 ppm$^2$). (2) Figure 7 assumes no additional local information (in the form of uncertain data) at the solution nodes. As a result, $f_G$ was conditioned only on the probabilistic datum at $\boldsymbol{p}_1$ = (0.1 km, 0.05 days), thus producing the twelve updated PDF $f_K$ shown in Figure 7. These PDF have distinct shapes across space and time. Also, some of them have very large widths (due to large standard deviations) and, as a result, their shapes are only partially displayed. In Figure 8 probabilistic data exist at two points in space/time, $\boldsymbol{p}_1$ = (0.3 km, 0.5 days) and $\boldsymbol{p}_2$ = (0.3 km, 2.0 days), whereas no additional soft data were assumed at the solution grid nodes. The resulting BME-based $f_K$ at four points are also shown in Figure 8.

[28] Given the $f_K$ of contaminant concentration across space/time we often seek particular forms of concentration values (realizations), such as the conditional mean, median or mode, depending on the application. The conditional mean (or BMEmean) at a point $\boldsymbol{p}_k$, e.g., is

$$\hat{\chi}_{k,mean} = \overline{X(\boldsymbol{p}_k)|\chi_{data}} = \int d\chi_k \chi_k f_K(\chi_k). \qquad (13)$$

For numerical illustration, BMEmean concentrations at all solution nodes of the space/time grid are plotted in Figure 9. Two cases are examined: (1) without additional soft data at the solution nodes and (2) with probabilistic data at the solution nodes. The plot of Figure 9a (case 1) depicts the effect on the prior concentration mean (plotted in Figure 3) of the site-specific knowledge at point $\boldsymbol{p}_1$. As was suggested in Figure 2, the low correlation between the soft datum point and remote solution nodes has a minimal effect on mean concentrations at the solution nodes $\boldsymbol{p}_k$. However, the

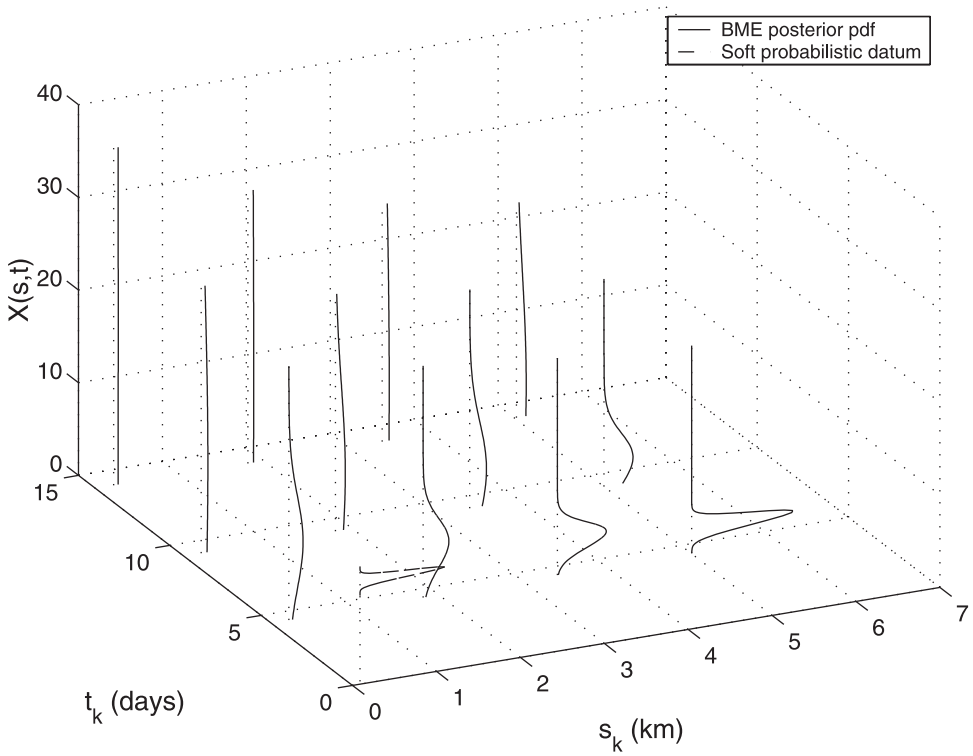


**Figure 7.** Probabilistic (soft) datum at point $\boldsymbol{p}_1$ = (0.1 *Km*, 0.05 *Days*) and the BME posterior PDF at several solution grid nodes.

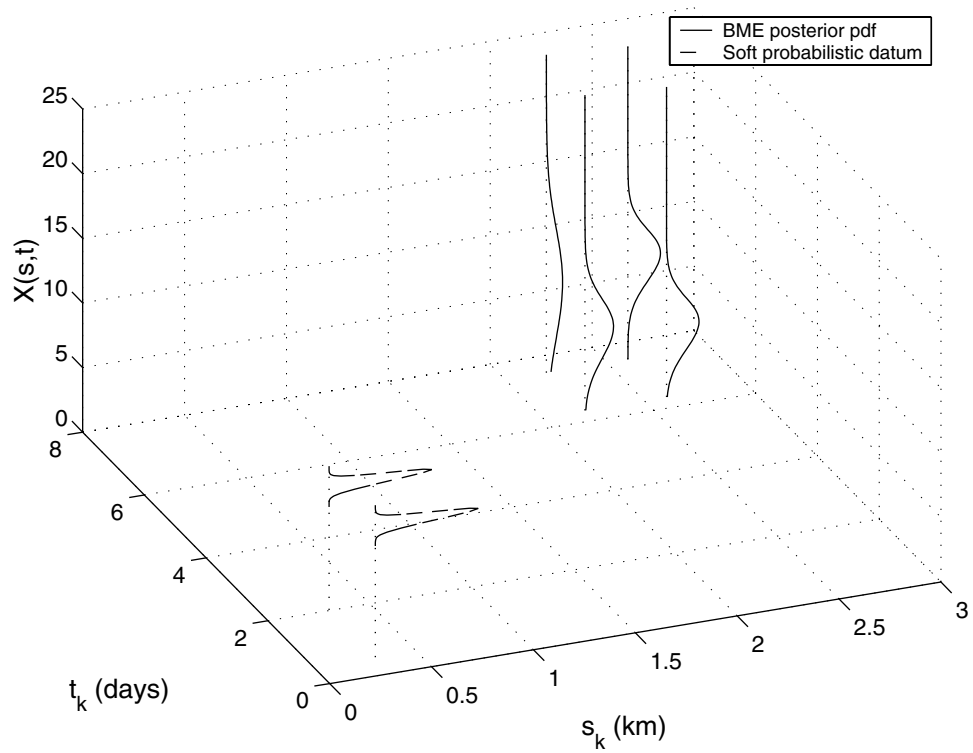


**Figure 8.** Probabilistic (soft) data at points $\boldsymbol{p}_1$ = (0.3 *Km*, 0.5 *Days*) and $\boldsymbol{p}_2$ = (0.3 *Km*, 2.0 *Days*) (no additional soft data are assumed at the solution grid nodes). The resulting BME posterior PDF at four solution nodes are also shown.

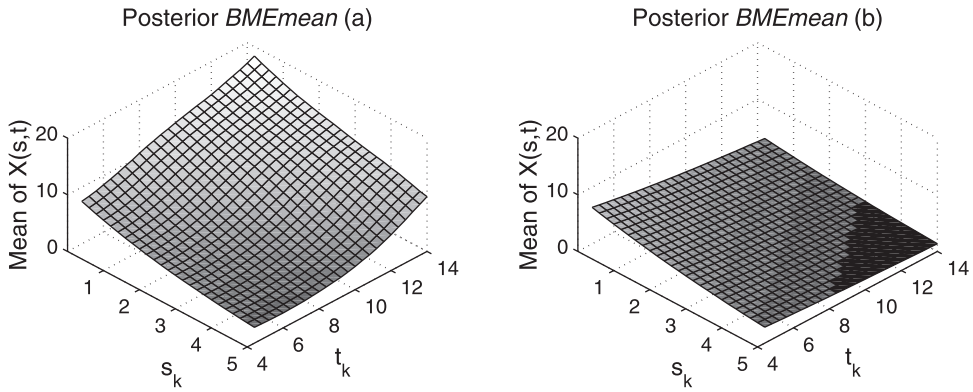


**Figure 9.** BME mean at solution grid nodes using a probabilistic datum at point $\boldsymbol{p}_1$ = (0.1 km, 0.05 days), (a) without any additional soft datum at the solution nodes and (b) in the presence of a second probabilistic datum at each solution node.

situation can change considerably when additional probabilistic (soft) data are introduced at the solution nodes $\boldsymbol{p}_k$ (case 2). In particular, Figure 10 depicts a series of PDF $f_K$ at the same solution nodes as in Figures 6 and 7, the difference being that probabilistic data are now assumed available at these nodes, as well. The combined effect on the BMEmean of the probabilistic datum at $\boldsymbol{p}_1$ and the additional probabilistic data at $\boldsymbol{p}_k$ is illustrated in Figure 9b. As a matter of fact, it turns out that the presence of even a small number of case-specific data enable BME to provide considerable information about the physical process in terms of the final solution ($f_K$). To our knowledge, no other stochastic method has so far been able to accommodate both a large collection of general knowledge bases and a rich variety of site-specific information bases in a scientifically rigorous framework, thus generating informative PDF of the contaminant variation across space and time.

[29] The computational BME technique implemented to solve the unsteady state, advection-reaction equation (1) in one spatial dimension can be extended without any conceptual difficulty to higher spatial dimensions. In the case, e.g., of a 2-D advection-reaction process, the $\mathbf{s} = (s_1, s_2)$ will denote the corresponding spatial coordinates, the scalar downstream velocity $q$ will be replaced by the flow velocity vector $\boldsymbol{q}$ and, as a result, the term $q\frac{\partial}{\partial s}$ will become $\boldsymbol{q} \cdot \nabla$. The structural PDF $f_G(\chi_i, \chi_j)$ for the pair of points ($\boldsymbol{p}_i$, $\boldsymbol{p}_j$) will be still given by equation (6). The coefficients $\mu_\alpha$ in equation (6) are now functions of 6 variables ($s_{1i}$, $s_{2i}$, $t_i$, $s_{1j}$,

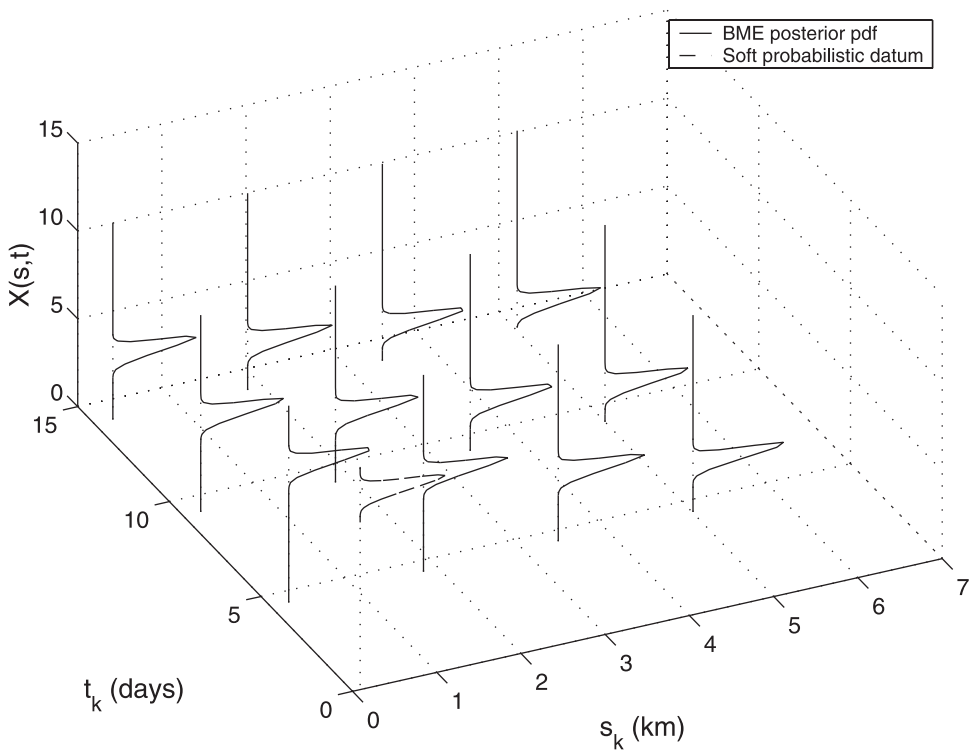


**Figure 10.** Probabilistic soft datum at point $\boldsymbol{p}_1$ = (0.1 km, 0.05 days) and the BME posterior PDF at several solution grid nodes with additional probabilistic data at the solution nodes.

$s_{2j}$, $t_j$) instead of 4, so that the corresponding discretization is a straightforward extension of that in Appendix C (i.e., from a 4-D to a 6-D stencil). Using the explicit scheme of this work, the numerical complexity increases linearly with the number of nodes so that the solution of the 2-D advection-reaction will require additional computational time but no major conceptual changes in the approach presented in the preceding sections will be necessary. Finally, the BME approach can be used in single-point or multipoint solution situations (i.e., one can produce univariate probability distributions at each solution node separately, as well as multivariate probability distributions at several space/time nodes simultaneously).

## 4. Discussion-Conclusions

[30] We have presented a novel computational technique for solving physical PDE in site-specific environments. The technique is based on the BME theory and it introduces solutions at every space/time point in the form of complete PDF, which do not only account for the physical law of interest but also for a host of other general and site-specific knowledge sources (often available in real world situations). More specifically, not only does the BME-based computational technique produce realistic maps across space and time by solving the stochastic law governing the underlying physical processes but, in addition, these maps can embody other forms of general knowledge (empirical charts, multiple-point statistics, constitutive relationships, etc.) as well as case-specific information (generated by a variety of measuring devices, including those involving considerable sources of uncertainty). Yet another advantage of the BME-based solution of a physical PDE over most standard PDE methods is that the former can improve the final solutions by incorporating uncertain information at the solution nodes themselves.

[31] We illustrated numerically the proposed technique in a contamination environment, which involved a representation of the advection-reaction process in terms of a PDE in space/time, the relevant boundary/initial conditions, and a set of hard data and soft concentration information (of the interval and the probabilistic types). We obtained numerical solutions for a system of nonlinear equations in 4 dimensions and introduced efficient ways to cope with complexity (due to higher dimensions) by observing the physics of the problem. Considering the space/time coordinates as separate but interacting subsystems for discretization purposes can be helpful in dealing with problems in higher dimensions (e.g., when investigating physical problems in 2 or 3 spatial dimensions plus time). The study was conducted in a controlled environment where the solution of the physical PDE was known in advance, thus allowing the evaluation of the proposed technique by comparing its solutions to the exact ones at the prior stage. No other numerical PDE techniques exists that share the salient features of the BME-based technique at the integration stage (e.g., accounting for various sorts of soft data at the solution nodes and uncertain observations at other locations, in addition to general knowledge in the form of physical law). As a result, our computational analysis at the integration stage cannot be easily compared to other numerical techniques for solving stochastic PDE.

[32] Certainly, in the majority of real world applications the analytical (exact) solution of the relevant physical PDE is not known. Even in those special cases in which explicit expressions are available, the existence of higher-order moments may create a complex environment. In the BME context, there is no need to explicitly solve the equation representing the physical law, since BME allows the information contained in the law to be consolidated implicitly into the general knowledge base considered at the structural (prior) stage. Therefore, in principle, BME poses no restrictions on the form of the physical equation or on the space/time pattern of the natural fields. However, as is the case with most numerical techniques, under certain circumstances (complex governing laws, highly involved expressions of observational uncertainty, etc.) a full numerical implementation of the proposed technique could be demanding in terms of computational resources. One of the directions of future work would focus on numerical issues related to more elaborate forms of general knowledge and site-specific data. Computationally, e.g., it should be more expensive to deal with higher-order multiple-point moments since both, the size of the nonlinear system will increase (to accommodate the extra moments and unknown Lagrange multipliers), and the integration order will increase by 1 for each additional point [*Hristopulos and Christakos*, 2001]. Investigations in code parallelization clearly suggested that further studies could benefit from the use of parallel processing. The promising results obtained so far imply that the numerical system of equations can be processed simultaneously at each grid node and multiple integrals calculations can be accelerated significantly, assuming the availability of high-quality multiprocessor hardware and the implementation of multipoint GQ integrations.

## Appendix A

[33] Assume that the physical constraints $\overline{g_a}$ include the mean $\overline{x_i} = \overline{X(\boldsymbol{p}_i)}$, the variance $\overline{x_i^2} = \overline{X^2(\boldsymbol{p}_i)}$ and the (non-centered) covariance $C_{ij} = \overline{X(\boldsymbol{p}_i)X(\boldsymbol{p}_j)}$ for all elements of the point vector $\boldsymbol{p}_{map}$. The corresponding $\overline{g_a}$ functions are as follows

$$\left.\begin{array}{ll} \overline{g_0(\boldsymbol{x}_{map})} = 1, & \overline{g_3(x_j)} = \overline{x_j} \\ \overline{g_1(x_i)} = \overline{x_i}, & \overline{g_4(x_j)} = \overline{x_j^2} \\ \overline{g_2(x_i)} = \overline{x_i^2}, & \overline{g_5(x_i,\, x_j)} = C_{ij} \end{array}\right\}, \tag{A1}$$

where $\overline{g_0(\boldsymbol{x}_{map})} = 1$ is the normalization constraint for the PDF $f_G$. Clearly, a different pair of points will be associated with a different set of functions $\overline{g_a}$. Taking into account the physical law (1), the associated functions $\overline{h_a}$ for any two points $\boldsymbol{p}_i$, $\boldsymbol{p}_j$ of the vector $\boldsymbol{p}_{map}$ will be

$$\left.\begin{array}{l} \overline{h_0(x_i,\, x_j)} = \int\int d\chi_i d\chi_j f_G(\chi_i, \chi_j) = 1 \\ \overline{h_1(x_i,\, x_j)} = -\kappa^{-1} \int\int d\chi_i\, d\chi_j\, \chi_i\, (\partial/\partial t_i + q\partial/\partial s_i) f_G \\ \overline{h_2(x_i,\, x_j)} = -(2\kappa)^{-1} \int\int d\chi_i\, d\chi_j\, \chi_i^2\, (\partial/\partial t_i + q\partial/\partial s_i) f_G \\ \overline{h_3(x_i,\, x_j)} = -\kappa^{-1} \int\int d\chi_i\, d\chi_j\, \chi_j\, (\partial/\partial t_j + q\partial/\partial s_j) f_G \\ \overline{h_4(x_i,\, x_j)} = -(2\kappa)^{-1} \int\int d\chi_i\, d\chi_j\, \chi_j^2\, (\partial/\partial t_j + q\partial/\partial s_j) f_G \\ \overline{h_5(x_i,\, x_j)} = -\kappa^{-1} \int\int d\chi_i\, d\chi_j\, \chi_i\, \chi_j\, (\partial/\partial t_i + q\partial/\partial s_i) f_G \end{array}\right\}, \tag{A2}$$

where $f_G = f_G(\chi_i, \chi_j; s_i, s_j, t_i, t_j)$, and assuming that the field $X(\boldsymbol{p})$ is differentiable in the mean square sense [*Christakos*, 1992]. By combining equations (A1) and (A2) we obtain the system of equation (5).

## Appendix B

[34] Given the first two moments of a bivariate random variable, the pdf that describes the variable is

$$f_G(\chi_i, \chi_j) = \frac{1}{2\pi|c_x|^{1/2}} \exp\left[-\frac{1}{2}(\boldsymbol{\chi} - \overline{\boldsymbol{x}})^T c_x^{-1}(\boldsymbol{\chi} - \overline{\boldsymbol{x}})\right], \quad \text{(B1)}$$

where $(\boldsymbol{\chi} - \overline{\boldsymbol{x}})^T = (\chi_i - \overline{x_i} \;\; \chi_j - \overline{x_j})$, and $\boldsymbol{c}_x = \begin{pmatrix} c_{ii} & c_{ij} \\ c_{ji} & c_{jj} \end{pmatrix}$ is the centered covariance matrix. It is required that

$$|c_x| = \begin{vmatrix} c_{ii} & c_{ij} \\ c_{ji} & c_{jj} \end{vmatrix} = \sigma_i^2\sigma_j^2 - c_{ij}c_{ji} \neq 0 \quad \text{(B2)}$$

The inverse of the covariance matrix $\boldsymbol{c}_x$ is

$$c_x^{-1} = \begin{pmatrix} c_{ii} & c_{ij} \\ c_{ji} & c_{jj} \end{pmatrix}^{-1} = \frac{1}{\sigma_i^2\sigma_j^2 - c_{ij}c_{ji}} \begin{pmatrix} c_{jj} & -c_{ij} \\ -c_{ji} & c_{ii} \end{pmatrix}. \quad \text{(B3)}$$

By expanding equation (B1) we regrouped the resulting terms with respect to $\chi_i$, $\chi_i^2$, $\chi_j$, $\chi_j^2$ and $\chi_i\chi_j$. Then, by comparing the terms of equation (B1) with those of equation (6) we can find the exact analytical expressions for the coefficients $\mu_\alpha(\boldsymbol{p}_i, \boldsymbol{p}_j)$, $\alpha = 0, 1, \ldots, N$ ($N = 5$, in this case). Note that as equation (8) suggests, the exact expressions for $\mu_\alpha(\boldsymbol{p}_i, \boldsymbol{p}_j)$ at each location $(s_i, t_i, s_j, t_j)$ are obtained by analytically calculating the means, variances, and covariances for that location. More specifically, we find

$$\begin{aligned}\overline{x_w} &= \overline{X(s_w, t_w)} \\ &= \exp[-\kappa t_w]\overline{X_0} \exp\left\{0.5\,(q\,t_w - s_w)\left[2\bar{c} + (q\,t_w - s_w)\sigma_c^2\right]\right\},\end{aligned} \quad \text{(B4)}$$

$$\begin{aligned}\sigma_w^2 &= \overline{X^2(s_w, t_w)} - \overline{x_w}^2 \\ &= \exp[-2\kappa t_w]\left(\sigma_{X_0}^2 + \overline{X_0}\right) \\ &\quad \cdot \exp\left\{2(q\,t_w - s_w)\left[\bar{c} + (q\,t_w - s_w)\,\sigma_c^2\right]\right\} - \overline{x_w}^2\end{aligned} \quad \text{(B5)}$$

for $w = i, j$, and

$$\begin{aligned}c_{ij} &= \overline{X(s_i, t_i)X(s_j, t_j)} - \overline{X(s_i, t_i)}\;\overline{X(s_j, t_j)} \\ &= \exp\left[-\kappa(t_i + t_j)\right]\left(\sigma_{X_0}^2 + \overline{X_0}\right) \\ &\quad \cdot \exp\left\{\frac{1}{2}\left[q(t_i + t_j) - (s_i + s_j)\right]\left[2\bar{c} + \left(q(t_i + t_j)\right.\right.\right. \\ &\quad \left.\left.\left. - (s_i + s_j)\right)\sigma_c^2\right]\right\} - \overline{x_i}\,\overline{x_j}.\end{aligned} \quad \text{(B6)}$$

In the previous calculations we have made use of the fact that the random variables $X_0$ and $c$ are independent, as well as the following relationship

$$\begin{aligned}\overline{\exp(Dc)} &= \int_{-\infty}^{\infty} dc\;\exp(Dc)\frac{1}{\sqrt{2\pi\sigma_c^2}}\exp\left[-\frac{(c - \bar{c})^2}{2\sigma_c^2}\right] \\ &= \exp\left[\frac{1}{2}D(2\bar{c} + D\sigma_c^2)\right],\end{aligned}$$

where $c$ is the random variable defined previously and $D$ is a constant. Note the exponential dependence of the mean and variance on the distribution of $c$. In section 2.5 we saw its significance in the evolution of $X(s, t)$ in space/time.

## Appendix C

[35] In the following the subscripts $r$ and $z$ refer to temporal and spatial grid nodes, respectively. The numerical solution of the equation system (5) involves three basic steps.

1. Consider the PDF $f_G(\chi_i, \chi_j)$ in equation (6) at times $t_i = t_{r_i+1}$ and $t_j = t_{r_j+1}$.
2. Expand the functions in equation (5) by discretizing the derivatives involved.
3. Calculate the Jacobian of the functions with respect to the coefficients $\mu_\alpha$, $\alpha = 0, 1, \ldots, N$ ($N = 5$, in this case).

[36] The system of equation (5) in step 1 gives

$$\begin{aligned}F_1(\chi_i, \chi_j) &= \int d\chi_j \int d\chi_i\chi_i\left(\frac{\partial}{\partial t_i} + q\frac{\partial}{\partial s_i} + \kappa\right) \\ &\quad \cdot \exp\left[\mu_{0z_i,z_j}^{r_i+1,r_j+1} + \mu_{1z_i,z_j}^{r_i+1,r_j+1}\chi_i + \mu_{2z_i,z_j}^{r_i+1,r_j+1}\chi_i^2\right. \\ &\quad \left.+\mu_{3z_i,z_j}^{r_i+1,r_j+1}\chi_j + \mu_{4z_i,z_j}^{r_i+1,r_j+1}\chi_j^2 + \mu_{5z_i,z_j}^{r_i+1,r_j+1}\chi_i\chi_j\right] = 0;\end{aligned} \quad \text{(C1a)}$$

$$\begin{aligned}F_2(\chi_i, \chi_j) &= \int d\chi_j \int d\chi_i\chi_i^2\left(\frac{\partial}{\partial t_i} + q\frac{\partial}{\partial s_i} + 2\kappa\right) \\ &\quad \cdot \exp\left[\mu_{0z_i,z_j}^{r_i+1,r_j+1} + \mu_{1z_i,z_j}^{r_i+1,r_j+1}\chi_i + \mu_{2z_i,z_j}^{r_i+1,r_j+1}\chi_i^2\right. \\ &\quad \left.+\mu_{3z_i,z_j}^{r_i+1,r_j+1}\chi_j + \mu_{4z_i,z_j}^{r_i+1,r_j+1}\chi_j^2 + \mu_{5z_i,z_j}^{r_i+1,r_j+1}\chi_i\chi_j\right] = 0;\end{aligned} \quad \text{(C1b)}$$

$$\begin{aligned}F_3(\chi_i, \chi_j) &= \int d\chi_j \int d\chi_i\chi_j\left(\frac{\partial}{\partial t_j} + q\frac{\partial}{\partial s_j} + \kappa\right) \\ &\quad \cdot \exp\left[\mu_{0z_i,z_j}^{r_i+1,r_j+1} + \mu_{1z_i,z_j}^{r_i+1,r_j+1}\chi_i + \mu_{2z_i,z_j}^{r_i+1,r_j+1}\chi_i^2\right. \\ &\quad \left.+\mu_{3z_i,z_j}^{r_i+1,r_j+1}\chi_j + \mu_{4z_i,z_j}^{r_i+1,r_j+1}\chi_j^2 + \mu_{5z_i,z_j}^{r_i+1,r_j+1}\chi_i\chi_j\right] = 0;\end{aligned} \quad \text{(C1c)}$$

$$\begin{aligned}F_4(\chi_i, \chi_j) &= \int d\chi_j \int d\chi_i\chi_j^2\left(\frac{\partial}{\partial t_j} + q\frac{\partial}{\partial s_j} + 2\kappa\right) \\ &\quad \cdot \exp\left[\mu_{0zi,z_j}^{r_i+1,r_j+1} + \mu_{1z_i,z_j}^{r_i+1,r_j+1}\chi_i + \mu_{2z_i,z_j}^{r_i+1,r_j+1}\chi_i^2\right. \\ &\quad \left.+\mu_{3z_i,z_j}^{r_i+1,r_j+1}\chi_j + \mu_{4z_i,z_j}^{r_i+1,r_j+1}\chi_j^2 + \mu_{5z_i,z_j}^{r_i+1,r_j+1}\chi_i\chi_j\right] = 0;\end{aligned} \quad \text{(C1d)}$$

and

$$\begin{aligned}F_5(\chi_i, \chi_j) &= \int d\chi_j \int d\chi_i\chi_i\chi_j\left(\frac{\partial}{\partial t_i} + q\frac{\partial}{\partial s_i} + \kappa\right) \\ &\quad \cdot \exp\left[\mu_{0z_i,z_j}^{r_i+1,r_j+1} + \mu_{1z_i,z_j}^{r_i+1,r_j+1}\chi_i + \mu_{2z_i,z_j}^{r_i+1,r_j+1}\chi_i^2\right. \\ &\quad \left.+\mu_{3z_i,z_j}^{r_i+1,r_j+1}\chi_j + \mu_{4z_i,z_j}^{r_i+1,r_j+1}\chi_j^2 + \mu_{5z_i,z_j}^{r_i+1,r_j+1}\chi_i\chi_j\right] = 0.\end{aligned} \quad \text{(C1e)}$$

For step 2, we use the first-order accurate Lax-Friedrichs scheme, according to which the temporal and spatial derivatives are approximated by, respectively,

$$\frac{\partial \mu}{\partial t} \cong \frac{\Delta \mu}{\Delta t} = \frac{\mu_z^{r+1} - \frac{1}{2}\left(\mu_{z+1}^r + \mu_{z-1}^r\right)}{\Delta t}, \text{ and } \frac{\partial \mu}{\partial s} \cong \frac{\Delta \mu}{\Delta s} = \frac{\mu_{z+1}^r - \mu_{z-1}^r}{2\ \Delta s}.$$

On the last spatial grid node the above derivatives can be approximated without the use of the unknown $\mu_{z+1}^r$, by substituting it, for example, with $\mu_z^r$. By applying the discretization scheme to equation (C1) we obtain, e.g., for $F_1(\chi_i, \chi_j; s_i, t_i, s_j, t_j)$:

$$\begin{aligned}
F_1(\chi_i,\chi_j) = \int d\chi_j \int d\chi_i \chi_i \ \exp\Big[ & \mu_{0z_i,z_j}^{r_i+1,r_j+1} + \mu_{1z_i,z_j}^{r_i+1,r_j+1}\chi_i \\
& + \mu_{2z_i,z_j}^{r_i+1,r_j+1}\chi_i^2 + \mu_{3z_i,z_j}^{r_i+1,r_j+1}\chi_j + \mu_{4z_i,z_j}^{r_i+1,r_j+1}\chi_j^2 \\
& + \mu_{5z_i,z_j}^{r_i+1,r_j+1}\chi_i\chi_j\Big]\Bigg(\frac{1}{\Delta t_i}\Bigg\{\Bigg[\mu_{0z_i,z_j}^{r_i+1,r_j} - \frac{1}{2}\left(\mu_{0z_i-1,z_j}^{r_i,r_j} + \mu_{0z_i-1,z_j}^{r_i,r_j}\right)\Bigg] \\
& + \chi_i\Bigg[\mu_{1z_i,z_j}^{r_i+1,r_j} - \frac{1}{2}\left(\mu_{1z_i+1,z_j}^{r_i,r_j} + \mu_{1z_i-1,z_j}^{r_i,r_j}\right)\Bigg] \\
& + \chi_i^2\Bigg[\mu_{2z_i,z_j}^{r_i+1,r_j} - \frac{1}{2}\left(\mu_{2z_i+1,z_j}^{r_i,r_j} + \mu_{2z_i-1,z_j}^{r_i,r_j}\right)\Bigg] \\
& + \chi_j\Bigg[\mu_{3z_i,z_j}^{r_i+1,r_j} - \frac{1}{2}\left(\mu_{3z_i+1,z_j}^{r_i,r_j} + \mu_{3z_i-1,z_j}^{r_i,r_j}\right)\Bigg] \\
& + \chi_j^2\Bigg[\mu_{4z_i,z_j}^{r_i+1,r_j} - \frac{1}{2}\left(\mu_{4z_i+1,z_j}^{r_i,r_j} + \mu_{4z_i-1,z_j}^{r_i,r_j}\right)\Bigg] \\
& + \chi_i\chi_j\Bigg[\mu_{5z_i,z_j}^{r_i+1,r_j} - \frac{1}{2}\left(\mu_{5z_i+1,z_j}^{r_i,r_j} + \mu_{5z_i-1,z_j}^{r_i,r_j}\right)\Bigg]\Bigg\} \\
& + \frac{q}{2\ \Delta s_i}\Bigg\{\left(\mu_{0z_i+1,z_j}^{r_i,r_j} - \mu_{0z_i-1,z_j}^{r_i,r_j}\right) + \chi_i\left(\mu_{1z_i+1,z_j}^{r_i,r_j} - \mu_{1z_i-1,z_j}^{r_i,r_j}\right) \\
& + \chi_i^2\left(\mu_{2z_i+1,z_j}^{r_i,r_j} - \mu_{2z_i-1,z_j}^{r_i,r_j}\right) + \chi_j\left(\mu_{3z_i+1,z_j}^{r_i,r_j} - \mu_{3z_i-1,z_j}^{r_i,r_j}\right) \\
& + \chi_j^2\left(\mu_{4z_i+1,z_j}^{r_i,r_j} - \mu_{4z_i-1,z_j}^{r_i,r_j}\right) + \chi_i\chi_j \\
& \left(\mu_{5z_i+1,z_j}^{r_i,r_j} - \mu_{5z_i-1,z_j}^{r_i,r_j}\right)\Bigg\} + \kappa\Bigg) = 0; \qquad \text{(C2a)}
\end{aligned}$$

$$\begin{aligned}
F_2(\chi_i,\chi_j) = \int d\chi_j \int d\chi_i \chi_i^2 \ \exp\Big[ & \mu_{0z_i,z_j}^{r_i+1,r_j+1} + \mu_{1z_i,z_j}^{r_i+1,r_j+1}\chi_i \\
& + \mu_{2z_i,z_j}^{r_i+1,r_j+1}\chi_i^2 + \mu_{3z_i,z_j}^{r_i+1,r_j+1}\chi_j + \mu_{4z_i,z_j}^{r_i+1,r_j+1}\chi_j^2 \\
& + \mu_{5z_i,z_j}^{r_i+1,r_j+1}\chi_i\chi_j\Big]\Bigg(\frac{1}{\Delta t_i}\Bigg\{\Bigg[\mu_{0z_i,z_j}^{r_i+1,r_j} - \frac{1}{2}\left(\mu_{0z_i+1,z_j}^{r_i,r_j} \\
& + \mu_{0z_i-1,z_j}^{r_i,r_j}\right)\Bigg] + \chi_i\Bigg[\mu_{1z_i,z_j}^{r_i+1,r_j} - \frac{1}{2}\left(\mu_{1z_i+1,z_j}^{r_i,r_j} + \mu_{1z_i-1,z_j}^{r_i,r_j}\right)\Bigg] \\
& + \chi_i^2\Bigg[\mu_{2z_i,z_j}^{r_i+1,r_j} - \frac{1}{2}\left(\mu_{2z_i+1,z_j}^{r_i,r_j} + \mu_{2z_i-1,z_j}^{r_i,r_j}\right)\Bigg] + \chi_j \\
& \cdot\Bigg[\mu_{3z_i,z_j}^{r_i+1,r_j} - \frac{1}{2}\left(\mu_{3z_i+1,z_j}^{r_i,r_j} + \mu_{3z_i-1,z_j}^{r_i,r_j}\right)\Bigg] + \chi_j^2 \\
& \cdot\Bigg[\mu_{4z_i,z_j}^{r_i+1,r_j} - \frac{1}{2}\left(\mu_{4z_i+1,z_j}^{r_i,r_j} + \mu_{4z_i-1,z_j}^{r_i,r_j}\right)\Bigg] + \chi_i\chi_j \\
& \cdot\Bigg[\mu_{5z_i,z_j}^{r_i+1,r_j} - \frac{1}{2}\left(\mu_{5z_i+1,z_j}^{r_i,r_j} + \mu_{5z_i-1,z_j}^{r_i,r_j}\right)\Bigg]\Bigg\} \\
& + \frac{q}{2\Delta s_i}\Bigg\{\left(\mu_{0z_i+1,z_j}^{r_i,r_j} - \mu_{0z_i-1,z_j}^{r_i,r_j}\right) + \chi_i\left(\mu_{1z_i+1,z_j}^{r_i,r_j} - \mu_{1z_i-1,z_j}^{r_i,r_j}\right) \\
& + \chi_i^2\left(\mu_{2z_i+1,z_j}^{r_i,r_j} - \mu_{2z_i-1,z_j}^{r_i,r_j}\right) + \chi_j\left(\mu_{3z_i+1,z_j}^{r_i,r_j} - \mu_{3z_i-1,z_j}^{r_i,r_j}\right) \\
& + \chi_j^2\left(\mu_{4z_i+1,z_j}^{r_i,r_j} - \mu_{4z_i-1,z_j}^{r_i,r_j}\right) + \chi_i\chi_j \\
& \left(\mu_{5z_i+1,z_j}^{r_i,r_j} - \mu_{5z_i-1,z_j}^{r_i,r_j}\right)\Bigg\} + \kappa\Bigg) = 0; \qquad \text{(C2b)}
\end{aligned}$$

$$\begin{aligned}
F_3(\chi_i,\chi_j) = \int d\chi_j \int d\chi_i \chi_j \ \exp\Big[ & \mu_{0z_i,z_j}^{r_i+1,r_j+1} + \mu_{1z_i,z_j}^{r_i+1,r_j+1}\chi_i \\
& + \mu_{2z_i,z_j}^{r_i+1,r_j+1}\chi_i^2 + \mu_{3z_i,z_j}^{r_i+1,r_j+1}\chi_j + \mu_{4z_i,z_j}^{r_i+1,r_j+1}\chi_j^2 \\
& + \mu_{5z_i,z_j}^{r_i+1,r_j+1}\chi_i\chi_j\Big]\Bigg(\frac{1}{\Delta t_j}\Bigg\{\Bigg[\mu_{0z_i,z_j}^{r_i,r_j+1} - \frac{1}{2}\left(\mu_{0z_i,z_j+1}^{r_i,r_j} \\
& + \mu_{0z_i,z_j-1}^{r_i,r_j}\right)\Bigg] + \chi_i\Bigg[\mu_{1z_i,z_j}^{r_i,r_j+1} - \frac{1}{2}\left(\mu_{1z_i,z_j+1}^{r_i,r_j} + \mu_{1z_i,z_j-1}^{r_i,r_j}\right)\Bigg] \\
& + \chi_i^2\Bigg[\mu_{2z_i,z_j}^{r_i,r_j+1} - \frac{1}{2}\left(\mu_{2z_i,z_j+1}^{r_i,r_j} + \mu_{2z_i,z_j-1}^{r_i,r_j}\right)\Bigg] + \chi_j \\
& \cdot\Bigg[\mu_{3z_i,z_j}^{r_i,r_j+1} - \frac{1}{2}\left(\mu_{3z_i,z_j+1}^{r_i,r_j} + \mu_{3z_i,z_j-1}^{r_i,r_j}\right)\Bigg] + \chi_j^2 \\
& \cdot\Bigg[\mu_{4z_i,z_j}^{r_i,r_j+1} - \frac{1}{2}\left(\mu_{4z_i,z_j+1}^{r_i,r_j} + \mu_{4z_i,z_j-1}^{r_i,r_j}\right)\Bigg] + \chi_i\chi_j \\
& \cdot\Bigg[\mu_{5z_i,z_j}^{r_i,r_j+1} - \frac{1}{2}\left(\mu_{5z_i,z_j+1}^{r_i,r_j} + \mu_{5z_i,z_j-1}^{r_i,r_j}\right)\Bigg]\Bigg\} \\
& + \frac{q}{2\Delta s_j}\Bigg\{\left(\mu_{0z_i,z_j+1}^{r_i,r_j} - \mu_{0z_i,z_j-1}^{r_i,r_j}\right) \\
& + \chi_i\left(\mu_{1z_i,z_j+1}^{r_i,r_j} - \mu_{1z_i,z_j-1}^{r_i,r_j}\right) + \chi_i^2\left(\mu_{2z_i,z_j+1}^{r_i,r_j} - \mu_{2z_i,z_j-1}^{r_i,r_j}\right) \\
& + \chi_j\left(\mu_{3z_i,z_j+1}^{r_i,r_j} - \mu_{3z_i,z_j-1}^{r_i,r_j}\right) + \chi_j^2\left(\mu_{4z_i,z_j+1}^{r_i,r_j} - \mu_{4z_i,z_j-1}^{r_i,r_j}\right) \\
& + \chi_i\chi_j\left(\mu_{5z_i,z_j+1}^{r_i,r_j} - \mu_{5z_i,z_j-1}^{r_i,r_j}\right)\Bigg\} + \kappa\Bigg) = 0; \qquad \text{(C2c)}
\end{aligned}$$

$$\begin{aligned}
F_4(\chi_i,\chi_j) = \int d\chi_j \int d\chi_i \chi_j^2 \ \exp\Big[ & \mu_{0z_i,z_j}^{r_i+1,r_j+1} + \mu_{1z_i,z_j}^{r_i+1,r_j+1}\chi_i \\
& + \mu_{2z_i,z_j}^{r_i+1,r_j+1}\chi_i^2 + \mu_{3z_i,z_j}^{r_i+1,r_j+1}\chi_j + \mu_{4z_i,z_j}^{r_i+1,r_j+1}\chi_j^2 \\
& + \mu_{5z_i,z_j}^{r_i+1,r_j+1}\chi_i\chi_j\Big]\Bigg(\frac{1}{\Delta t_j}\Bigg\{\Bigg[\mu_{0z_i,z_j}^{r_i,r_j+1} - \frac{1}{2}\left(\mu_{0z_i,z_j+1}^{r_i,r_j} \\
& + \mu_{0z_i,z_j-1}^{r_i,r_j}\right)\Bigg] + \chi_i\Bigg[\mu_{1z_i,z_j}^{r_i,r_j+1} - \frac{1}{2}\left(\mu_{1z_i,z_j+1}^{r_i,r_j} + \mu_{1z_i,z_j-1}^{r_i,r_j}\right)\Bigg] \\
& + \chi_i^2\Bigg[\mu_{2z_i,z_j}^{r_i,r_j+1} - \frac{1}{2}\left(\mu_{2z_i,z_j+1}^{r_i,r_j} + \mu_{2z_i,z_j-1}^{r_i,r_j}\right)\Bigg] + \chi_j
\end{aligned}$$

$$\cdot\left[\mu_{3z_i,z_j}^{r_i,r_j+1}-\frac{1}{2}\left(\mu_{3z_i,z_j+1}^{r_i,r_j}+\mu_{3z_i,z_j-1}^{r_i,r_j}\right)\right]+\chi_j^2$$
$$\cdot\left[\mu_{4z_i,z_j}^{r_i,r_j+1}-\frac{1}{2}\left(\mu_{4z_i,z_j+1}^{r_i,r_j}+\mu_{4z_i,z_j-1}^{r_i,r_j}\right)\right]+\chi_i\chi_j$$
$$\cdot\left[\mu_{5z_i,z_j}^{r_i,r_j+1}-\frac{1}{2}\left(\mu_{5z_i,z_j+1}^{r_i,r_j}+\mu_{5z_i,z_j-1}^{r_i,r_j}\right)\right]\Bigg\}$$
$$+\frac{q}{2\Delta s_j}\Bigg\{\left(\mu_{0z_i,z_j+1}^{r_i,r_j}-\mu_{0z_i,z_j-1}^{r_i,r_j}\right)\chi_i\left(\mu_{1z_i,z_j+1}^{r_i,r_j}-\mu_{1z_i,z_j-1}^{r_i,r_j}\right)$$
$$+\chi_i^2\left(\mu_{2z_i,z_j+1}^{r_i,r_j}-\mu_{2z_i,z_j-1}^{r_i,r_j}\right)+\chi_j\left(\mu_{3z_i,z_j+1}^{r_i,r_j}-\mu_{3z_i,z_j-1}^{r_i,r_j}\right)$$
$$+\chi_j^2\left(\mu_{4z_i,z_j+1}^{r_i,r_j}-\mu_{4z_i,z_j-1}^{r_i,r_j}\right)+\chi_i\chi_j\Bigg(\mu_{5z_i,z_j+1}^{r_i,r_j}$$
$$-\mu_{5z_i,z_j-1}^{r_i,r_j}\Bigg)\Bigg\}+2\kappa\Bigg)=0; \tag{C2d}$$

$$F_5(\chi_i,\chi_j)=\int d\chi_j\int d\chi_i\,\chi_i\chi_j\,\exp\Bigg[\mu_{0z_i,z_j}^{r_i+1,r_j+1}+\mu_{1z_i,z_j}^{r_i+1,r_j+1}\chi_i$$
$$+\mu_{2z_i,z_j}^{r_i+1,r_j+1}\chi_i^2+\mu_{3z_i,z_j}^{r_i+1,r_j+1}\chi_j+\mu_{4z_i,z_j}^{r_i+1,r_j+1}\chi_j^2$$
$$+\mu_{5z_i,z_j}^{r_i+1,r_j+1}\chi_i\chi_j\Bigg]\Bigg(\frac{1}{\Delta t_i}\Bigg\{\left[\mu_{0z_i,z_j}^{r_i+1,r_j}-\frac{1}{2}\left(\mu_{0z_i+1,z_j}^{r_i,r_j}\right.\right.$$
$$\left.\left.+\mu_{0z_i-1,z_j}^{r_i,r_j}\right)\right]+\chi_i\left[\mu_{1z_i,z_j}^{r_i+1,r_j}-\frac{1}{2}\left(\mu_{1z_i+1,z_j}^{r_i,r_j}+\mu_{1z_i-1,z_j}^{r_i,r_j}\right)\right]$$
$$+\chi_i^2\left[\mu_{2z_i,z_j}^{r_i+1,r_j}-\frac{1}{2}\left(\mu_{2z_i+1,z_j}^{r_i,r_j}+\mu_{2z_i-1,z_j}^{r_i,r_j}\right)\right]$$
$$+\chi_j\left[\mu_{3z_i,z_j}^{r_i+1,r_j}-\frac{1}{2}\left(\mu_{3z_i+1,z_j}^{r_i,r_j}+\mu_{3z_i-1,z_j}^{r_i,r_j}\right)\right]$$
$$+\chi_j^2\left[\mu_{4z_i,z_j}^{r_i+1,r_j}-\frac{1}{2}\left(\mu_{4z_i+1,z_j}^{r_i,r_j}+\mu_{4z_i-1,z_j}^{r_i,r_j}\right)\right]$$
$$+\chi_i\chi_j\left[\mu_{5z_i,z_j}^{r_i+1,r_j}-\frac{1}{2}\left(\mu_{5z_i+1,z_j}^{r_i,r_j}+\mu_{5z_i-1,z_j}^{r_i,r_j}\right)\right]\Bigg\}$$
$$+\frac{q}{2\Delta s_i}\Bigg\{\left(\mu_{0z_i+1,z_j}^{r_i,r_j}-\mu_{0z_i-1,z_j}^{r_i,r_j}\right)+\chi_i\left(\mu_{1z_i+1,z_j}^{r_i,r_j}-\mu_{1z_i-1,z_j}^{r_i,r_j}\right)$$
$$+\chi_i^2\left(\mu_{2z_i+1,z_j}^{r_i,r_j}-\mu_{2z_i-1,z_j}^{r_i,r_j}\right)+\chi_j\left(\mu_{3z_i+1,z_j}^{r_i,r_j}-\mu_{3z_i-1,z_j}^{r_i,r_j}\right)$$
$$+\chi_j^2\left(\mu_{4z_i+1,z_j}^{r_i,r_j}-\mu_{4z_i-1,z_j}^{r_i,r_j}\right)+\chi_i\chi_j\Bigg(\mu_{5z_i+1,z_j}^{r_i,r_j}$$
$$-\mu_{5z_i-1,z_j}^{r_i,r_j}\Bigg)\Bigg\}+\kappa\Bigg)=0. \tag{C2e}$$

Equations (C1b)–(C1e) are discretized in a similar way. Finally, in stage C we obtain the components of the Jacobian

$$J(\boldsymbol{F},\boldsymbol{\mu})=\partial\boldsymbol{F}(\boldsymbol{\chi};\boldsymbol{\mu})/\partial\boldsymbol{\mu}\Big|_{\substack{t_{r_i+1},t_{r_j+1}\\ s_{z_i},s_{z_j}}} \tag{C3}$$

$$=\begin{pmatrix}
\frac{\partial F_1(\boldsymbol{\chi};\boldsymbol{\mu})}{\partial\mu_{1z_i,z_j}^{r_i+1,r_j+1}} & \frac{\partial F_1(\boldsymbol{\chi};\boldsymbol{\mu})}{\partial\mu_{2z_i,z_j}^{r_i+1,r_j+1}} & \frac{\partial F_1(\boldsymbol{\chi};\boldsymbol{\mu})}{\partial\mu_{3z_i,z_j}^{r_i+1,r_j+1}} & \frac{\partial F_1(\boldsymbol{\chi};\boldsymbol{\mu})}{\partial\mu_{4z_i,z_j}^{r_i+1,r_j+1}} & \frac{\partial F_1(\boldsymbol{\chi};\boldsymbol{\mu})}{\partial\mu_{5z_i,z_j}^{r_i+1,r_j+1}}\\
\frac{\partial F_2(\boldsymbol{\chi};\boldsymbol{\mu})}{\partial\mu_{1z_i,z_j}^{r_i+1,r_j+1}} & \frac{\partial F_2(\boldsymbol{\chi};\boldsymbol{\mu})}{\partial\mu_{2z_i,z_j}^{r_i+1,r_j+1}} & \frac{\partial F_2(\boldsymbol{\chi};\boldsymbol{\mu})}{\partial\mu_{3z_i,z_j}^{r_i+1,r_j+1}} & \frac{\partial F_2(\boldsymbol{\chi};\boldsymbol{\mu})}{\partial\mu_{4z_i,z_j}^{r_i+1,r_j+1}} & \frac{\partial F_2(\boldsymbol{\chi};\boldsymbol{\mu})}{\partial\mu_{5z_i,z_j}^{r_i+1,r_j+1}}\\
\frac{\partial F_3(\boldsymbol{\chi};\boldsymbol{\mu})}{\partial\mu_{1z_i,z_j}^{r_i+1,r_j+1}} & \frac{\partial F_3(\boldsymbol{\chi};\boldsymbol{\mu})}{\partial\mu_{2z_i,z_j}^{r_i+1,r_j+1}} & \frac{\partial F_3(\boldsymbol{\chi};\boldsymbol{\mu})}{\partial\mu_{3z_i,z_j}^{r_i+1,r_j+1}} & \frac{\partial F_3(\boldsymbol{\chi};\boldsymbol{\mu})}{\partial\mu_{4z_i,z_j}^{r_i+1,r_j+1}} & \frac{\partial F_3(\boldsymbol{\chi};\boldsymbol{\mu})}{\partial\mu_{5z_i,z_j}^{r_i+1,r_j+1}}\\
\frac{\partial F_4(\boldsymbol{\chi};\boldsymbol{\mu})}{\partial\mu_{1z_i,z_j}^{r_i+1,r_j+1}} & \frac{\partial F_4(\boldsymbol{\chi};\boldsymbol{\mu})}{\partial\mu_{2z_i,z_j}^{r_i+1,r_j+1}} & \frac{\partial F_4(\boldsymbol{\chi};\boldsymbol{\mu})}{\partial\mu_{3z_i,z_j}^{r_i+1,r_j+1}} & \frac{\partial F_4(\boldsymbol{\chi};\boldsymbol{\mu})}{\partial\mu_{4z_i,z_j}^{r_i+1,r_j+1}} & \frac{\partial F_4(\boldsymbol{\chi};\boldsymbol{\mu})}{\partial\mu_{5z_i,z_j}^{r_i+1,r_j+1}}\\
\frac{\partial F_5(\boldsymbol{\chi};\boldsymbol{\mu})}{\partial\mu_{1z_i,z_j}^{r_i+1,r_j+1}} & \frac{\partial F_5(\boldsymbol{\chi};\boldsymbol{\mu})}{\partial\mu_{2z_i,z_j}^{r_i+1,r_j+1}} & \frac{\partial F_5(\boldsymbol{\chi};\boldsymbol{\mu})}{\partial\mu_{3z_i,z_j}^{r_i+1,r_j+1}} & \frac{\partial F_5(\boldsymbol{\chi};\boldsymbol{\mu})}{\partial\mu_{4z_i,z_j}^{r_i+1,r_j+1}} & \frac{\partial F_5(\boldsymbol{\chi};\boldsymbol{\mu})}{\partial\mu_{5z_i,z_j}^{r_i+1,r_j+1}}
\end{pmatrix}.$$

As an example, the derivative of $F_1(\chi_i, \chi_j; s_i, t_i, s_j, t_j)$ with respect to $\mu_1(s_i, t_i, s_j, t_j)$ follows

$$\frac{\partial F_1(\chi;\mu)}{\partial\mu_{1z_i,z_j}^{r_i+1,r_j+1}}=\int d\chi_j\int d\chi_i\chi_i^2\exp\Bigg(\mu_{0z_i,z_j}^{r_i+1,r_j+1}+\mu_{1z_i,z_j}^{r_i+1,r_j+1}\chi_i$$
$$+\mu_{2z_i,z_j}^{r_i+1,r_j+1}\chi_i^2+\mu_{3z_i,z_j}^{r_i+1,r_j+1}\chi_j+\mu_{4z_i,z_j}^{r_i+1,r_j+1}\chi_j^2$$
$$+\mu_{5z_i,z_j}^{r_i+1,r_j+1}\chi_i\chi_j\Bigg)\Bigg(\frac{1}{\Delta t_i}\Bigg\{1+\left[\mu_{0z_i,z_j}^{r_i+1,r_j}-\frac{1}{2}\left(\mu_{0z_i+1,z_j}^{r_i,r_j}\right.\right.$$
$$\left.\left.+\mu_{0z_i-1,z_j}^{r_i,r_j}\right)\right]+\chi_i\left[\mu_{1z_i,z_j}^{r_i+1,r_j}-\frac{1}{2}\left(\mu_{1z_i+1,z_j}^{r_i,r_j}+\mu_{1z_i-1,z_j}^{r_i,r_j}\right)\right]$$
$$+\chi_i^2\left[\mu_{2z_i,z_j}^{r_i+1,r_j}-\frac{1}{2}\left(\mu_{2z_i+1,z_j}^{r_i,r_j}+\mu_{2z_i-1,z_j}^{r_i,r_j}\right)\right]+\chi_j$$
$$\cdot\left[\mu_{3z_i,z_j}^{r_i+1,r_j}-\frac{1}{2}\left(\mu_{3z_i+1,z_j}^{r_i,r_j}+\mu_{3z_i-1,z_j}^{r_i,r_j}\right)\right]+\chi_j^2$$
$$\cdot\left[\mu_{4z_i,z_j}^{r_i+1,r_j}-\frac{1}{2}\left(\mu_{4z_i+1,z_j}^{r_i,r_j}+\mu_{4z_i-1,z_j}^{r_i,r_j}\right)\right]+\chi_i\chi_j$$
$$\cdot\left[\mu_{5z_i,z_j}^{r_i+1,r_j}-\frac{1}{2}\left(\mu_{5z_i+1,z_j}^{r_i,r_j}+\mu_{5z_i-1,z_j}^{r_i,r_j}\right)\right]\Bigg\}$$
$$+\frac{q}{2\,\Delta s_i}\Bigg\{\left(\mu_{0z_i+1,z_j}^{r_i,r_j}-\mu_{0z_i-1,z_j}^{r_i,r_j}\right)+\chi_i\left(\mu_{1z_i+1,z_j}^{r_i,r_j}-\mu_{1z_i-1,z_j}^{r_i,r_j}\right)$$
$$+\chi_i^2\left(\mu_{2z_i+1,z_j}^{r_i,r_j}-\mu_{2z_i-1,z_j}^{r_i,r_j}\right)+\chi_j\left(\mu_{3z_i+1,z_j}^{r_i,r_j}-\mu_{3z_i-1,z_j}^{r_i,r_j}\right)$$
$$+\chi_j^2\left(\mu_{4z_i+1,z_j}^{r_i,r_j}-\mu_{4z_i-1,z_j}^{r_i,r_j}\right)+\chi_i\chi_j$$
$$\cdot\left(\mu_{5z_i+1,z_j}^{r_i,r_j}-\mu_{5z_i-1,z_j}^{r_i,r_j}\right)\Bigg\}+\kappa\Bigg). \tag{C4}$$

The remaining Jacobian discretized components are obtained in a similar manner.

[37] **Acknowledgments.** This work has been supported by grants from the National Institute of Environmental Health Sciences (grant P42 ES05948-02) and the U.S. Civilian Research and Development Foundation (grant RJ2-2236).

## References

Adler, P. M., *Porous Media, Geometry and Transport*, Butterworth-Heinemann, Boston, Mass., 1992.

Atkinson, K. E., *An Introduction to Numerical Analysis*, John Wiley, New York, 1989.

Christakos, G., A Bayesian/maximum entropy view to the spatial estimation problem, *Math. Geol.*, *22*(7), 763–777, 1990.

Christakos, G., Some applications of the Bayesian maximum-entropy concept in geostatistics, in *Maximum Entropy and Bayesian Methods*, edited by W. T. Grandy Jr. and L. H. Schick, pp. 215–229, Kluwer Acad., Norwell, Mass., 1991.

Christakos, G., *Random Field Models in Earth Sciences*, Academic, San Diego, Calif., 1992.

Christakos, G., Spatiotemporal information systems in soil and environmental sciences, *Geoderma*, *85*(2–3), 141–179, 1998.

Christakos, G., *Modern Spatiotemporal Geotatistics*, Oxford Univ. Press, New York, 2000.

Christakos, G., and D. T. Hristopulos, *Spatiotemporal Environmental Health Modelling: A Tractatus Stochasticus*, Kluwer Acad., Norwell, Mass., 1998.

Christakos, G., D. T. Hristopulos, and M. L. Serre, BME studies of stochastic differential equations representing physical laws, part I, in *Proceedings of IAMG '99: Fifth Annual Conference of the International Association for Mathematical Geology*, vol. 1, edited by S. J. Lippard, A. Naess, and R. Sinding-Larsen, pp. 63–68, Norw. Univ. of Sci. and Technol., Trondheim, Norway, 1999.

Conte, S. D., and C. De Boor, *Elementary Numerical Analysis: An Algorithmic Approach*, 3rd ed., 432 pp., McGraw-Hill, New York, 1980.

Dale, V. H., and M. R. English, *Tools to Aid Environmental Decision Making*, Springer-Verlag, New York, 1999.

Department of Defense, Groundwater Modelling System, Hydraul. Lab., U. S. Army Eng. Waterw. Exp. Stn., Washington, D. C., 1997.

Farthing, M. W., and C. T. Miller, A comparison of high-resolution, finite-volume, adaptive-stencil schemes for simulating advective-dispersive transport, *Adv. Water Res.*, *24*, 29–48, 2000.

Flaherty, J. E., P. J. Paslow, M. S. Shephard, and J. D. Vasilakis, *Adaptive Methods for Partial Differential Equations*, Soc. for Ind. and Appl. Math, Philadelphia, Pa., 1989.

Goldberg, M. A., *Solution Methods for Integral Equations*, Plenum, New York, 1979.

Gropp, W., E. Lusk, and A. Skjellum, *Using MPI: Portable Parallel Programming With the Message-Passing Interface*, 2nd ed., 371 pp., MIT Press, Cambridge, Mass., 1999.

Hristopulos, D. T., and G. Christakos, Practical calculation of non-Gaussian multivariate moments in BME analysis, *Math. Geol.*, *33*(5), 543–568, 2001.

Javandel, I., C. Doughty, and C. F. Tsang, *Groundwater Transport: Handbook of Mathematical Models*, *Water Resour. Monogr. Ser.*, vol. 10, AGU, Washington, D. C., 1984.

Jordan, D. W., and P. Smith, *Nonlinear Ordinary Differential Equations*, Oxford Univ. Press, New York, 1987.

Kitanidis, P. K., Parameter uncertainty in estimation of spatial functions: Bayesian analysis, *Water Resour. Res.*, *22*, 449–507, 1986.

Knox, R. C., D. A. Sabatini, and L. W. Canter, *Subsurface Transport and Fate Processes*, A. F. Lewis, Boca Raton, Fla., 1993.

Lapidus, L., and G. F. Pinder, *Numerical Solution of Partial Differential Equations in Science and Engineering*, John Wiley, New York, 1982.

McCormick, S. F., *Multigrid Methods*, Soc. for Ind. and Appl. Math, Philadelphia, Pa., 1987.

Mynett, A. E., Hydroinformatics and its applications at Delft hydraulics, *J. Hydroinf.*, *1*(2), 83–102, 1999.

Nocedal, J., and S. J. Wright, *Numerical Optimization*, Springer-Verlag, New York, 1999.

Ortega, J. M., and W. C. Rheinboldt, *Iterative Solution of Non-linear Equations in Several Variables*, Academic, San Diego, Calif., 1982.

Papoulis, A., *Probability, Random Variables, and Stochastic Processes*, 3rd. ed., McGraw-Hill, New York, 1991.

Schnoor, J., *Environmental Modeling: Fate and Transport of Pollutants in Water, Air and Soil*, John Wiley, New York, 1996.

Serre, M. L., and G. Christakos, BME studies of stochastic differential equations representing physical laws, part II, in *Proceedings of IAMG '99: Fifth Annual Conference of the International Association for Mathematical Geology*, vol. 1, edited by S. J. Lippard, A. Naess, and R. Sinding-Larsen, pp. 93–98, Norw. Univ. of Sci. and Technol., Trondheim, Norway, 1999.

Smith, B., P. Bjørstad, and W. Gropp, *Domain Decomposition*, Cambridge Univ. Press, New York, 1996.

Spitz, K., and J. Moreno, *A Practical Guide to Groundwater and Solute Transport Modeling*, John Wiley, New York, 1996.

Srinivasan, S. K., and R. Vasudevan, *Introduction to Random Differential Equations and Their Applications*, Elsevier Sci., New York, 1971.

Steinberg, L. J., K. H. Reckhow, and R. L. Wolpert, Bayesian model for fate and transport of polychlorinated biphenyl in upper Hudson river, *J. Environ. Eng.*, *122*(5), 341–349, 1996.

Strikwerda, J., *Finite Difference Schemes and Partial Differential Equation*, Chapman and Hall, New York, 1989.

Weber, W. J., Jr., and F. A. DiGiano, *Process Dynamics in Environmental Systems*, John Wiley, New York, 1996.

Zhang, D., *Stochastic Methods for Flow in Porous Media*, Academic, San Diego, Calif., 2002.

G. Christakos, A. Kolovos, C. T. Miller, and M. L. Serre, Center for the Advanced Study of the Environment, University of North Carolina at Chapel Hill, Chapel Hill, NC 27599-7431, USA. (george_christakos@unc.edu)